



CO₂ capturing in cross T-junction microchannel using numerical and experimental approach

Bushra Khatoon¹ · Shabih Ul Hasan¹ · M. Siraj Alam¹

Received: 16 February 2023 / Accepted: 21 June 2023 / Published online: 5 July 2023
© Institute of Chemistry, Slovak Academy of Sciences 2023

Abstract

Numerical and experimental studies were carried out for the analysis of hydrodynamics and volumetric mass transfer coefficient ($k_L a$) in a cross-T junction microchannel for gas–liquid, two phase flow system. Initially, CO₂–water hydrodynamics simulation was performed using ANSYS-FLUENT 2021 R2 and volume of fluid technique. Through the numerical simulation, fluctuation in pressure drop with variation in volume fraction was calculated for the slug flow in a 1 mm hydraulic diameter microchannel. After that mass transfer equations were coupled with the flow equations for CO₂–ethyl glycol, CO₂–water, and CO₂–ethyl alcohol systems to understand the mass transfer mechanism using two film theory concepts. Computational fluid dynamics model was validated by comparing results with the experimental data. An empirical co-relation was also developed to measure the bubble length with its position in the direction of fluid flow. CO₂ and solvents velocities were 0.21–0.424 m/s for both the phase. Effect of solvents and film thickness (0.01–0.05 mm) on volumetric mass transfer coefficient were investigated at different temperatures range i.e., T = 298.15 K and 303.15 K (experimental approach) and 298.15–318.15 K (numerical approach). The results obtained in numerical simulation and experimental work show that the total volumetric mass transfer coefficient (range 0.1–0.8 1/s) increases with the gas velocity however, it decreases with increasing film thickness (0.01–0.05 mm) and temperature (T = 298.15 K and 303.15 K). The present work gives an advantage over the conventional channel (e.g., packed bed column) and the other type of T-junction microchannel (e.g., symmetric T-junction) by providing a high mixing rate, interfacial area, and high mass transfer rate.

Keywords Hydrodynamics · Microchannel · Physical absorption · Mass transfer coefficient · Slug flow

List of Symbols

u	Velocity of the fluid (m/s)
P	Pressure (Pa)
T	Temperature (K)
F	Body force (N/m ³)
C	Concentration (mol/m ³)
D	Diffusion coefficient (m ² /s)
R	Rate of gas absorption (mole/m ³ s)
k	Mass transfer coefficient (m/s)
V	Volume (m ³)
a	Specific area (m ² /m ³)
x	Position (mm)
L	Length of the bubble (mm)
t	Time (s)

Greek letters

α	Volume fraction of fluid (dimensionless)
ρ	Density of the fluid (kg/m ³)
μ	Viscosity of the fluid (Pa s)
σ	Surface tension (N/m)
κ	Surface curvature (mm)
δ	Film thickness (mm)

Subscripts

L	Liquid phase
G	Gas phase
i	Species
s	Superficial
B	Bubble
$G0$	At the initial condition

Abbreviations

CFD	Computational fluid dynamics
CSF	Continuum surface force
VOF	Volume of fluid

✉ M. Siraj Alam
msalam@mnnit.ac.in

¹ Chemical Engineering Department, Motilal Nehru National Institute of Technology-Allahabad, Prayagraj, U.P. 211004, India

Introduction

Through time people are progressively shifting their life towards industrialization and operating such industries entails a lot of energy. To attain a huge amount of energy the big resource is the combustion of fossil fuel (Mahmoudi Marjanian et al. 2021; Aghel et al. 2018). With instant advantages of these industries like refineries, coal fire-power plants, transportation, etc., are responsible for the present as well as the future condition of the environment (Aghel et al. 2018; Davison 2007; Guo et al. 2020) where acid gases (Kundu and Bandyopadhyay 2006) becoming the major origin of the numerous difficulties around the world. From prior literature data and the factual observations that give information about the recent state of the atmosphere such as a rapid change in climate (Tan et al. 2012; Buckingham et al. 2021), the rise of earth's temperature due to greenhouse gases (Wang et al. 2021), and solution to the control this problem is the major concern of the researchers (Ochedi et al. 2020; Ahmed et al. 2020). The composition of greenhouse gases is Carbon dioxide, Methane, Nitrous oxide (Extavour and Bunje 2016), Water vapor (Modak and Jana 2018), and Fluorinated gases (Yoro and Daramola 2020) which CO₂ is highly responsible for the major environmental problem.

According to Energy Agency (IEA 2022), the concentration of CO₂ emission ranges to the average value of 412.5 ppm in 2020, and the climate service of India (IMD 2022) reported the effect of CO₂ emission on the temperature rise and divergence in rainfall is represented in Fig. 1.

Furthermore, researchers have suggested several techniques and methods that are represented in Fig. 2. For separation/capturing of CO₂ like absorption (Lee et al. 2013), adsorption (Ahmed et al. 2020; Bhowm and Freeman 2011), cryogenic (Göttlicher and Pruschek 1997), and membrane (Leung et al. 2014; Kenarsari et al. 2013), and calcium looping (Criado et al. 2017) use in conventional equipment (Rouzitalab et al. 2020; Zhang et al. 2016) that provide effective results (Mukherjee et al. 2019; Bonaventura et al. 2017).

For the different ranges of temperatures (Gul 2022), pressures (Khan et al. 2017), and gas absorption is the most utilized and promising method that can be used to capture or separate CO₂ (Ye et al. 2013). Removal of CO₂ can be enhanced by providing sufficient contact time and interface area by the use of different solvents like Water (Zunlong et al. 2021), NH₃ (Liu et al. 2009), H₂S (Huang et al. 2017), KOH (Rastegar and Ghaemi 2022), NaOH (Krauß and Rzehak 2017), Na₂CO₃ (Rodríguez-Mosqueda et al. 2018) or Na₂CO₃ integrated with CaCO₃ (Barzagli et al. 2017), Alcohols (Gui et al. 2011), Amines (Simons et al. 1975; Adak et al. 2020), Glycols (Hayduk and Malik 1971), Nanofluids

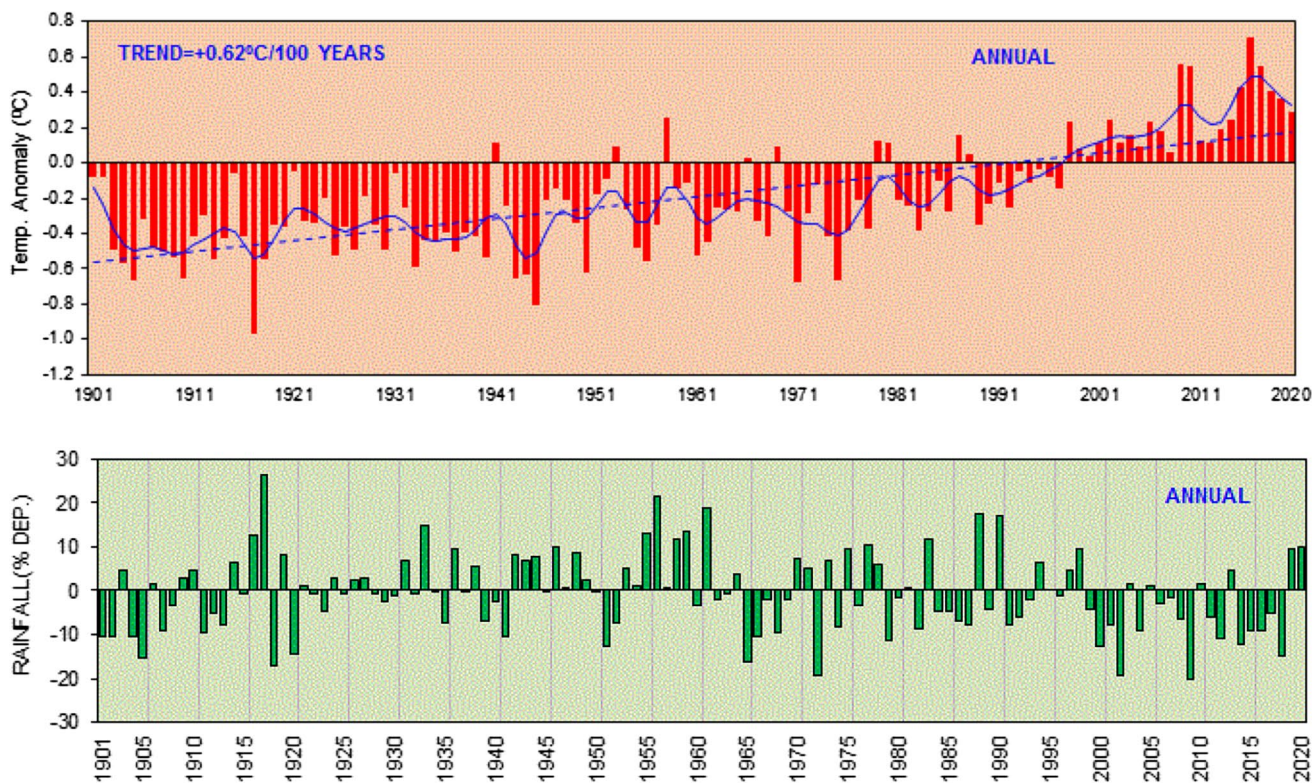


Fig. 1 Anomaly time series of temperature (°C) and rainfall (%depth) reported by IMD Ministry of Earth Sciences

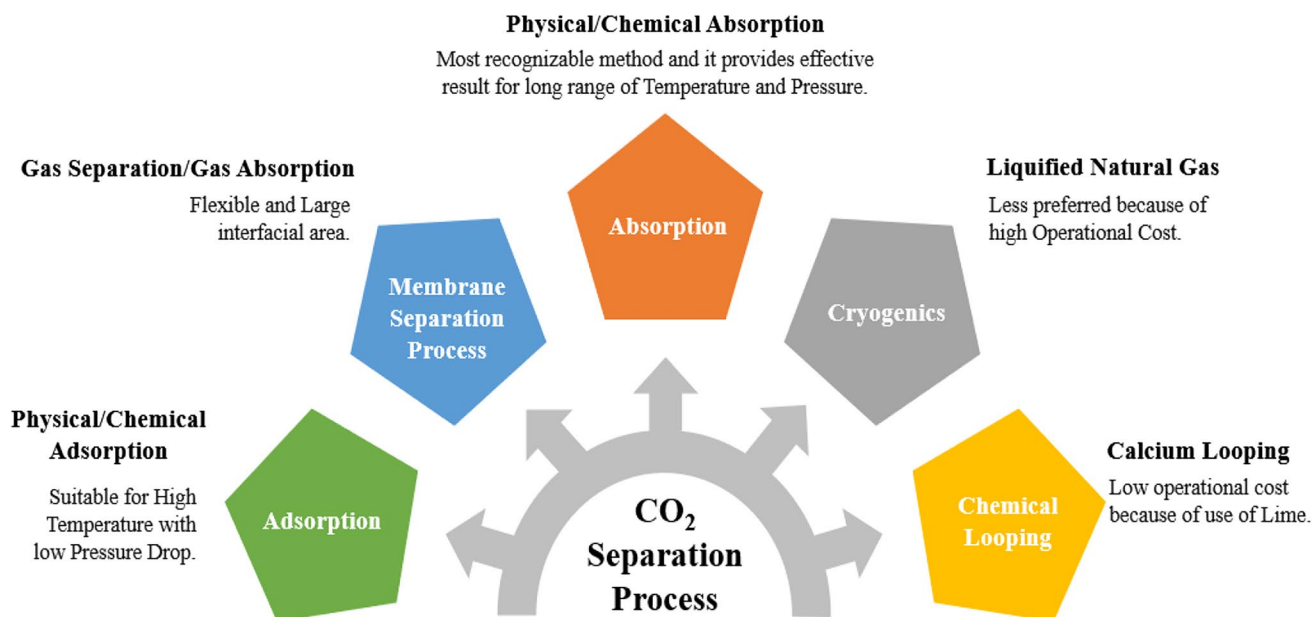


Fig. 2 CO₂ separation processes are broadly categorized as adsorption, membrane-separations, cryogenics, calcium looping, and absorption

(Zhang et al. 2018), Ionic fluids (Ramdin et al. 2012), equipment other than conventional channels e.g., mini/microfluidic-devices (Khatoon et al. 2022; Yao et al. 2014; Kuhn and Jensen 2012) using experimental (Ghadyanlou et al. 2022) and numerical method (Harkou et al. 2021; Li et al. 2022).

Microfluidics is the most advanced term in the field of research and technology. At the beginning of this field, its applications were limited to the heat transfer (Tuckerman and Pease 1981) purpose but in recent times it has had several applications [hydrodynamics (Khan et al. 2018; Chandra et al. 2016), high rate of heat (Chandra et al. 2015), and mass transfer (Pohar and Plazl 2009; Chen et al. 2008; Kenig et al. 2013), good reaction control (Renken and Kiwi-Minsker 2010)] in the different areas like process industries (Pua and Rumbold 2003; Palo et al. 2006), biomedical (King 2006), pharmaceuticals (Huang et al. 2019), emulsification (Ganguli and Pandit 2021), and electronics (Dix and Jokar 2018), etc.

On the other hand, geometrical representation is also an important characteristic that plays a very vital role in the two-phase flow system. A vast study of literature (Ansari et al. 2010; Venkateshwarlu and Bharti 2023; Boruah et al. 2018; Liu et al. 2016) reported that 1–1 cross-T microfluidic junction (less costly and low maintenance required) gives a higher rate of mixing (Santos and Kawaji 2011; Qian and Lawal 2006) for two-phase flow system (Sarkar et al. 2014; Mastiani et al. 2017). Two-phase separation phenomena are affected by the different parameters i.e., diameter of the main arm, diameter ratio (side arm to the main arm), inclination of the main arm, inclination of sidearm, radius of curvature, outlet inclination, flow regime, pressure drops (during phase

separation), densities of phases, mass split ratio, gas/liquid superficial velocities, and flow regime in the main pipe (Ejazi et al. 2021).

From the study of several kinds of literature (Ni et al. 2017; Dong and Hibiki 2018; Kreutzer et al. 2005; Lim et al. 2019), it is found that in microchannels different types of flow patterns like annular, bubbly, slug (Chaoqun et al. 2013), churn, wavy, etc. (Triplett et al. 1999; Bordbar et al. 2018), can be obtained with the variation in the fluid velocities. Fluctuations in flow rate create vibrations in the pipes with rising velocities of gas at a constant liquid flow rate flow pattern shifted from plug to slug flow. It was seen that slug flow appeared for a wide range of velocities/flow rates (Yin 2022) with the high-pressure fluctuation in the T-junction. To maintain the constant slug length in the channels it is necessary to choose the accurate inner diameter of the channels and fluid flow rates may also have a small effect on its stability (Kang et al. 2021).

In the present work to capture/separate the CO₂, cross-T junction microfluidic equipment, slug flow, with the absorption method was used but the selection of the solvents was the main challenge for this study. The purpose of the recent work is the minimization of the processing cost and use of energy (energy consumed to recover or regenerate the costly solvents) by the utilization of physical solvents i.e., water, glycols, and alcohols. Physical solvents drop the chances of microchannels from getting blocked and their limit can be pulled beyond the limit of chemical solvents.

A numerical gas–liquid-based model was developed for the current work and compared with the experimental observations at two different temperatures in a cross-T-junction

microchannel. Obtained results are related to the hydrodynamics and mass transfer study and are associated with the literature data for the conventional channel as well. An attempt is made the development of empirical co-relation for the measurement of bubble length. In conventional, mini, and microchannels it was found that microchannels offer high CO₂ capturing rate with the physical absorption method at a particular combination of gas and liquid phase velocities.

Material and methods

Computational approach

In the present study, computational fluid dynamics (CFD) numerical simulation was performed using the finite volume method with the help of the ANSYS 2021 R2 platform. The volume of fluid (VOF) is an Eulerian method that is the most renowned, reliable, and numerically expensive technique to track the interphase for the study of multiphase flow system (Nekouei and Vanapalli 2017; Chiriac et al. 2022). Here, the VOF method was used for the analysis of a two-phase (gas–liquid) flow system, a cross-T-junction in which gas enters through the side arm, liquid enters from the main arm, and Taylor/slug flow is observed in the running arm.

Hydrodynamic model

Two-dimensional (2D) Laminar fluid flow for CO₂-different solvents is considered for the present work with the following assumptions:

1. Newtonian and incompressible fluid
2. Gravity effect is not considered (due to the small horizontal channel with a small diameter i.e., mm)
3. Geometry is not responsible for the change in the physical properties of the fluid
4. No slip condition considered at the wall

5. Marangoni effect is neglected so the surface tension remains constant during fluid flow in the microchannel

Detail description of geometry

Here, the 2D cross-T junction geometry selected for the present study has two inlets (at 90°), with 1 mm hydraulic diameter, one outlet with 1 mm hydraulic diameter, length of the main arm, side arm, and running arms are 3 mm, 3 mm, and 47 mm respectively. This geometry (Fig. 3) was created using ANSYS 2021 R2 design modular (DM).

Volume of fluid (VOF) method

The volume of fluid is a numerical technique that is used in literature for the analysis of the interface between two or more phase flow simply and economically. This method helps to find out the continuity of the surface, the physical properties of the fluid at the chosen surface, and tangential velocities (Hirt and Nichols 1981). Basic equations that were used in this method is written in the form of volume fraction (α) which play an important role in tracking the interface between two/multiphase system.

Governing equations

The following equations are written for each phase of two flow systems according to the present work (Khan et al. 2018):

$$\alpha_L + \alpha_G = 1 \quad (1)$$

$$\rho = \rho_G + (\rho_L - \rho_G)\alpha_L \quad (2)$$

$$\mu = \mu_G + (\mu_L - \mu_G)\alpha_L \quad (3)$$

where ρ_L , ρ_G , μ_L , and μ_G are the density and viscosity of gas and liquid phase respectively, while α_G is the volume fraction of gas. Based the local value of α_G the appropriate properties and variables will be assigned to each control volume within the domain.

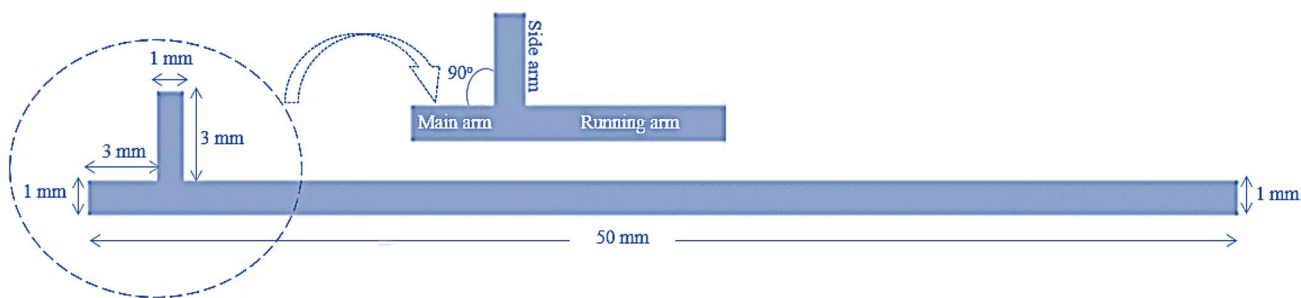


Fig. 3 Schematic representation of cross-T junction microchannel

Continuity equation

$$\frac{\partial}{\partial t}(\rho_i \alpha_i) + \nabla \cdot (\rho_i \alpha_i \vec{u}_i) = 0 \tag{4}$$

For incompressible fluid the above equations can be rewritten for a two-phase flow system as follows (Chandra et al. 2016):

$$\frac{\partial}{\partial t}(\alpha_L) + \nabla \cdot (\vec{u}_L \alpha_L) = 0 \tag{5}$$

$$\frac{\partial}{\partial t}(\alpha_G) + \nabla \cdot (\vec{u}_G \alpha_G) = 0 \tag{6}$$

Navier–Stokes equation

Navier Stokes equation was coupled with the continuity equation, VOF method, and with the body force, \vec{F} is body force that shows the combined effect of surface tension as well as interfacial properties (Liu et al. 2016).

$$\frac{\partial}{\partial t}(\rho \vec{u}) + \nabla \cdot (\rho \vec{u} \vec{u}) = -\nabla P + (\mu(\nabla^2 \vec{u}) + \vec{F}) \tag{7}$$

$$\vec{F} = \frac{2\rho\sigma\kappa\nabla\alpha}{\rho_L + \rho_G} \tag{8}$$

where u is used for the velocity of the fluid, σ is surface tension, κ is surface curvature, and P represents the pressure (Pham et al. 2012).

Mass transfer equation:

In gas–liquid microchannels available interfacial surface area enhances the mass transfer rate several times (Khan et al. 2021) by utilizing the absorption concept in the slug flow pattern. A generalized transport equation used for the mass transfer of gas into liquid is mentioned below (Zunlong

et al. 2021; Yao et al. 2014; Yang et al. 2014; Makarem et al. 2021):

$$\rho \frac{\partial C_i}{\partial t} + \vec{u} \cdot \nabla C_i = \rho D_i \nabla^2 C_i + R_i \tag{9}$$

Two film theory mass transfer models were used to track the movement of gas molecules into the liquid through the interface (Baten and Krishna 2004) (Fig. 4).

$$R_i = k_G(P_i^{Bulk} - P_i^{Interface}) = k_L(C_i^{Interface} - C_i^{Bulk}) \tag{10}$$

where C is concentration, D is diffusion coefficient, R is the rate of gas absorption, and k is the mass transfer coefficient at a given temperature.

Boundary conditions

All the information that was required for the recent model and the values were considered in ANSYS FLUENT 2021 R2 with the inlet, outlet, and surface boundary conditions listed in Tables 1 and 2 respectively.

Selection of mesh size and grid independency test

Selection of an exactly suitable grid was quite challenging and it took a lot of time to choose the optimum result for a recent study. It's really necessary to predict the degree of accuracy to justify the consequential decision. After several trials with the size of elements, it was gained around 0.6 million nodes, fluctuation in the pressure and slug length became constant at the precise position of the microchannel, Fig. 5.

Quadrilateral, uniform, and structured mesh type was used to study hydrodynamics in cross-T junction microchannel, Fig. 6. For the mass transfer observation, unstructured (useful for complex geometry for arbitrary position) and the quadrilateral mesh were employed for the reason of the bubble shape, Fig. 7.

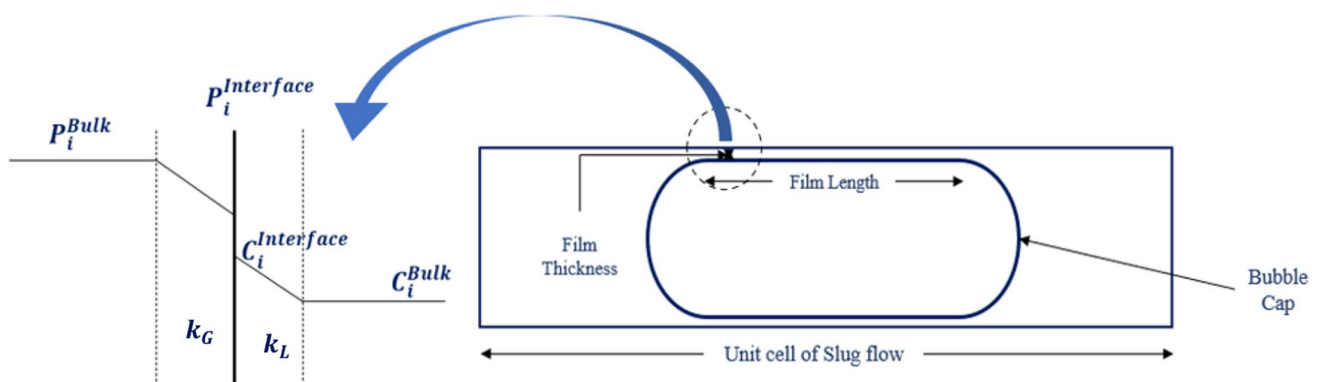


Fig. 4 Interfacial representation of Taylor bubble and liquid slug using two film theories

Table 1 Model, methods, and initialization conditions for the present work (Fluent Theory Guide 2013)

Model	
Viscous model	Laminar
Multiphase Model	
Number of Eulerian phases	2 for each case
Volume fraction formulation	Explicit
Body force formulation	Implicit body force
Interface modelling	Sharp
Courant number	0.25
Modelling of surface tension	CSF (Brackbill et al. 1992)
Methods	
Pressure–velocity coupling	PISO
Pressure	
Momentum	PRESTO
Volume fraction	Second order upwind
Geo reconstructs	
Initialization	
Initialization methods	Standard
Gauge pressure	
Velocity	0 Pa
The volume fraction of Liquid	0.424 m/s
The volume fraction of Gas	1
$0 < \alpha < 1$	0
	Interphase

Experimental approach

The gas–liquid operation was executed for the study of hydrodynamics and mass transfer in the laboratory in the cross-T junction (Fig. 8), with the similar geometry that was explained (used for numerical approach) in section of computational approach. To perform the experiments, a micro-reactor setup was purchased from Amar Equipment Pvt. Ltd. Kurla Mumbai, India. This set up consists two peristaltic pumps, microchannel or microreactor, camera, sensors, MFC's to control the fluid flow, control panel, beakers, and data acquisition system.

In this experiment, fluid flow data is inserted with the help of computer programme. As per given instructions to the computer, gas introduced in to one inlet and the solvent from the other inlet with the help of peristaltic

pump. First step was related to the hydrodynamics of the CO₂–water system to check out the range where Taylor/slug flow can be obtained. Once slug flow pattern was attained at a particular combination of velocity for a diffusing system (CO₂–water), this velocity data was utilized for the study of hydrodynamics and mass transfer study of the other diffusing system i.e., CO₂–ethyl alcohol and CO₂–glycols. Mixture of gas–liquid system was collected in a beaker from the outlet of cross T-junction. For the present work, solvents were chosen with physical absorption criteria, no reactions were considered for both (numerical and experimental) approaches.

An online method (Yao et al. 2014) was used to calculate the mass transfer coefficient values from the experimental data for each diffusive system and validated with numerical results. As the CO₂ started to absorb in the liquid, the size of the bubble ongoing to shrink. The mass transfer rate from a gaseous phase to the liquid phase for the unit slug length (Fig. 9) can be calculated from the following equation:

$$\frac{dV_G}{dx} U_G = -k_L a (C_G - C^0) \frac{V_L RT}{P} \quad (11)$$

The volumetric mass transfer coefficient ($k_L a$) was obtained from the equation that is mentioned below (Yue et al. 2007):

$$k_L a = \frac{u_s}{x} \ln \left(\frac{C_{G,0} - C^0}{C_G - C^0} \right) \quad (12)$$

By solving Eqs. 11 and 12, the length of the bubble (gaseous phase) can be expressed in terms of bubble position i.e., x (Eq. 13):

$$L_G = a + b \cdot \exp(-c \cdot x) \quad (13)$$

where expansion of a, b, and c are listed below:

$$a = L_{G0} - \frac{(C_{G,0} - C^0)}{U_G \cdot A_G} \cdot \frac{V_L RT u_s}{P}, \quad (14)$$

$$b = \frac{(C_{G,0} - C^0)}{u_G \cdot A_G} \cdot \frac{V_L RT u_s}{P} \quad (15)$$

Table 2 Initial boundary condition for each system in the cross-T junction microchannel

Number of cases	Systems	Boundary condition		
		Inlet 1	Inlet 2	Outlet
		Flow rate (ml/min)	Flow rate (ml/min)	Pressure (kPa)
Case 1	CO ₂ + water	10	20	101.325
Case 2	CO ₂ + ethyl alcohol	10	20	101.325
Case 3	CO ₂ + ethyl glycol	10	20	101.325

Fig. 5 Diagram shows the effect of the number of nodes on the slug length and pressure drop (GIT)

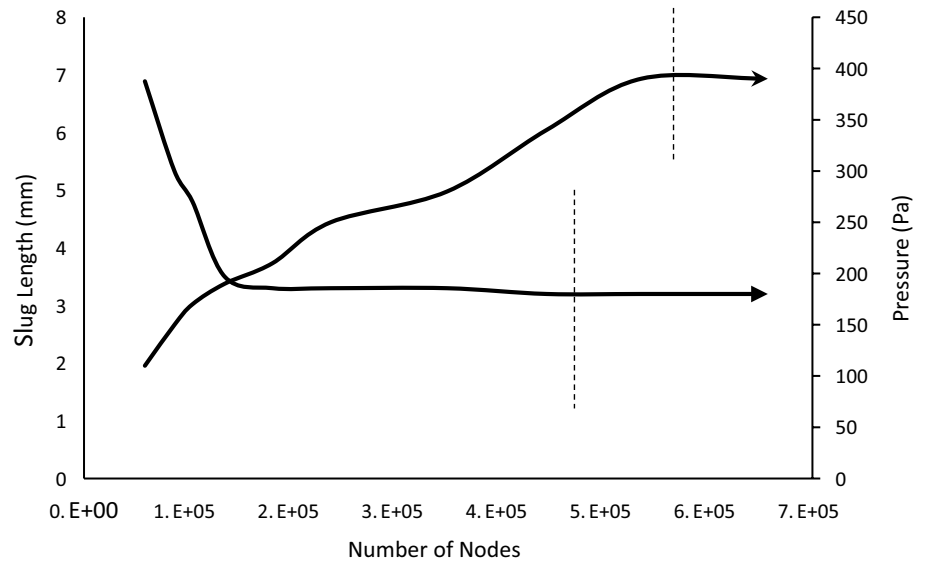


Fig. 6 Representation of meshed geometry i.e., cross-T junction

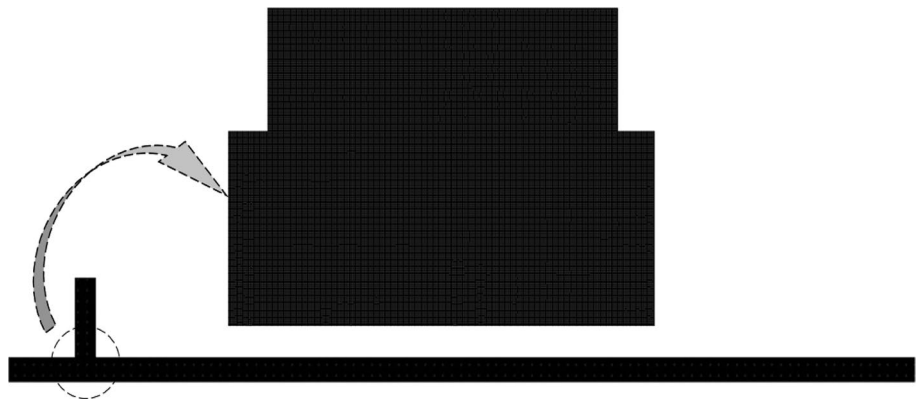
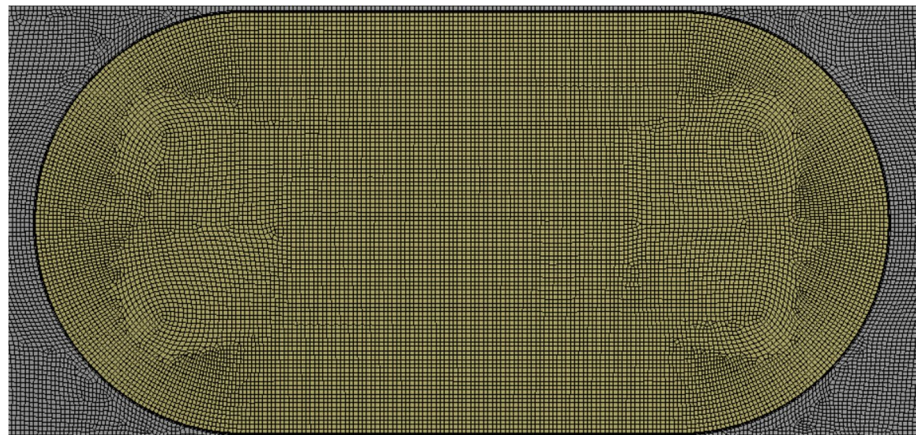


Fig. 7 Representation of unstructured meshed Taylor bubble inside the microchannel (running arm)



$$c = \frac{k_L a}{u_s} \tag{16}$$

It was considered overall volumetric mass transfer coefficient ($k_L a$) is a combination of the film bubble length side

($k_L a_{FilmBubbleLengthSide}$) and film bubble cap side volumetric mass transfer coefficient ($k_L a_{FilmBubbleCapSide}$), Eqs. 17, and 18 (Zunlong et al. 2021).

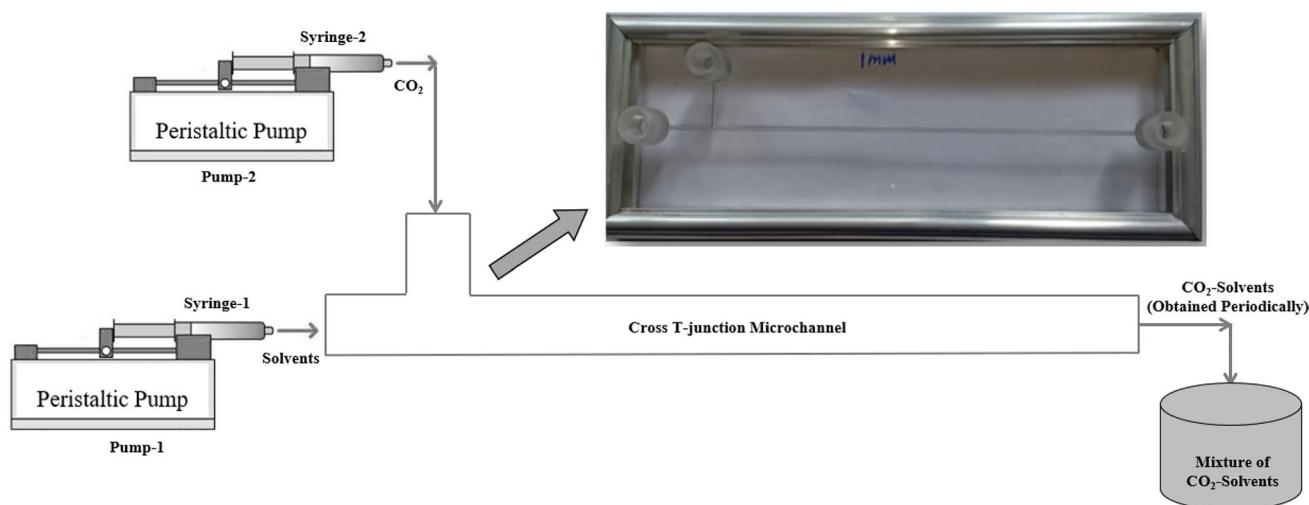


Fig. 8 Schematic image of experimental set up and cross-T junction (hydraulic dia = 1 mm) used in the laboratory

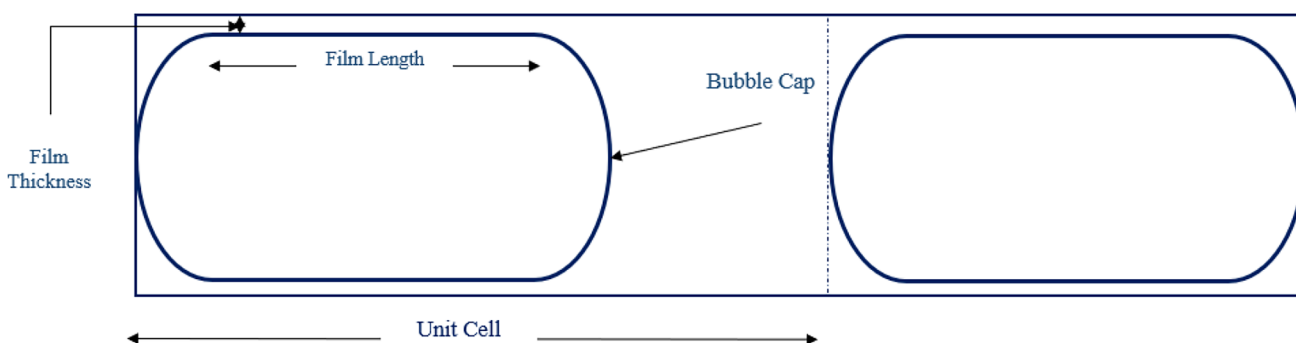


Fig. 9 Schematic representation of unit slug length

$$k_L a = k_L a_{\text{FilmBubbleLengthSide}} + k_L a_{\text{FilmBubbleCapSide}} \quad (17)$$

$$k_L a_{\text{Film}} = \frac{D_{GL}}{\delta} \quad (18)$$

Study of solvent performance

In the literature, several solvents give good solubility of CO_2 without chemical reactions. The selection of solvent in the physical absorption process is an important criterion that highly depends on the functional group (OH, COO, C=O, –O–), temperature, and pressure (Gui et al. 2011; Simons et al. 1975). For the present study water, ethyl alcohol, and ethyl glycol were chosen solvents to capture the CO_2 in the cross-T junction microchannel, listed in Table 3. The physical properties of all fluid are in mentioned Tables 4 and 5.

Results and discussion

To understand the performance of any equipment and transport phenomena characteristics it is always necessary to went through a detailed study of the hydrodynamics (change in velocities, pressure fluctuation) in that equipment. So, one can enhance the optimization condition of the system. In the present work, a hydrodynamic model was developed for case 1 with the help of continuity and Navier Stokes equation using the VOF method and obtained slug/Taylor flow for a wide range of velocities in the microchannels. After that developed model was used for the numerical simulation of case 1, 2, and case 3, obtained results were compared with experimental data. A mass transfer study is also performed to obtain the volumetric mass transfer coefficient value and also checked the effect of gas velocities, and bubble length on this parameter.

Table 3 A selected gas–liquid system for the recent study

System	Mass transfer process
CO ₂ + water	Physical absorption
CO ₂ + ethyl alcohol	Physical absorption
CO ₂ + Ethyl glycol	Physical absorption

Table 4 Physical properties of the fluid at different temperature (Gui et al. 2011; Hayduk and Malik 1971; Yao et al. 2014; Snijder et al. 1996)

Ambient temperature (K)	Fluid	Density (kg/m ³)	Viscosity × 10 ⁻³ (Pa.s)	Surface Tension (N/m)
298.15	CO ₂	1.833	6.97	–
	Water	998	1.003	0.0727
	Ethyl alcohol	791	1.189	0.0223
	Ethyl glycol	1109.8	17.01	0.0473
303.15	CO ₂	1.78	1.793	–
	Water	995.65	0.798	0.0712
	Ethyl alcohol	784	1.023	0.216
	Ethyl glycol	1102.5	16.58	0.0469

Hydrodynamics study for CO₂–water system

Effect of velocity

On the several variations in the velocity range (0.2–0.5) of the two-phase flow system i.e., gas (CO₂) and water (H₂O), we have obtained a Taylor bubble flow pattern in the microchannel at $u_G = 0.2$ m/s and $u_L = 0.4$ m/s, Fig. 10. It was observed that the length of the bubble and slug have higher dimensions than the diameter of the microchannel and the interfacial area in the slug flow pattern (Fig. 10c) is much higher than the other two fluid flow patterns (Fig. 10a, b).

Mixing velocity enhances approx. 6 folds at the cross-T-junction and each slug have high average velocity and circulation rate than the Taylor bubble (Fig. 11).

Table 5 Physical properties of the fluid at temperature 298.15 K (Zunlong et al. 2021; Gui et al. 2011; Snijder et al. 1996; Souvignet and Olesik 1998)

Parameters	
Velocity range (m/s)	0.2–0.5
Diffusivity (m ² /s)	CO ₂ + water $D_{CO_2-H_2O} = 2.35 \times 10^{-6} \exp\left(\frac{-2119}{T}\right)$
	CO ₂ + ethyl alcohol $D_{CO_2-alcohol} = 3.336 \times 10^{-6} \exp\left(\frac{-2119}{T}\right)$
	CO ₂ + ethyl glycol 0.279×10^{-9} (at 298.15 K), 0.285×10^{-9} (at 303.15 K)
Temperature (K)	298.15, and 303.15
Film thickness range (mm), film length (mm)	0.01–0.05, 4.5

Study of two-phase pressure drop in a microchannel

Because of the complicated behaviour of the two-phase flow system in microchannels, it is quite difficult to observe the pressure fluctuations. ANSYS FLUENT provides the platform for the study of pressure drop fluctuation at each point inside the microchannel. It was observed high-pressure fluctuation at the cross-T junction due to high mixing velocity (Fig. 12). The value of pressure was high inside the bubble than the slug, and bubble cap due to Laplace pressure which is also mentioned by different scholars (Yao et al. 2014; Abadie et al. 2012).

Change in volume fraction in the direction of flow

In the volume of fluid (VOF) method, the volume fraction (α) term is used to define the fluid phase and interface study. Figure 13 is a volume fraction plot that shows the variation for each phase at an interface in slug fluid flow with a repeated pattern between 0 and 1 values. In the plot, solid line was used for single phases and dotted lines represent interphase between the CO₂–water system.

For detailed tracking of volume fraction, $x = 19$ mm position was selected and endeavored to observe the movement of the bubble through this position with the time that is mentioned in Fig. 14.

In Fig. 14, it can be clearly seen that the vertical dotted line (probe) inside the running arm of microchannel, at time (t) = 0 s the only water was present there and as time passes this liquid was pushed by a bubble in the direction of flow. With the movement of fluid, in the first step water moves along the channel length with a defined position ($x = 19$ mm), after that interface comes in contact with the probe (dotted line), and then bubble crosses over there.

Figure 15 gives data about the change of the volume fraction in a unit cell and it can be seen the α value is 1 for water, which started to decrease with time and this value tends to decrease towards 0 that means only bubble is present in time span $t = 0.05$ – 0.1 s. After that α value started to increase reaches to 1 which means again water

Fig. 10 CO₂–water phase contour at different combinations of velocities

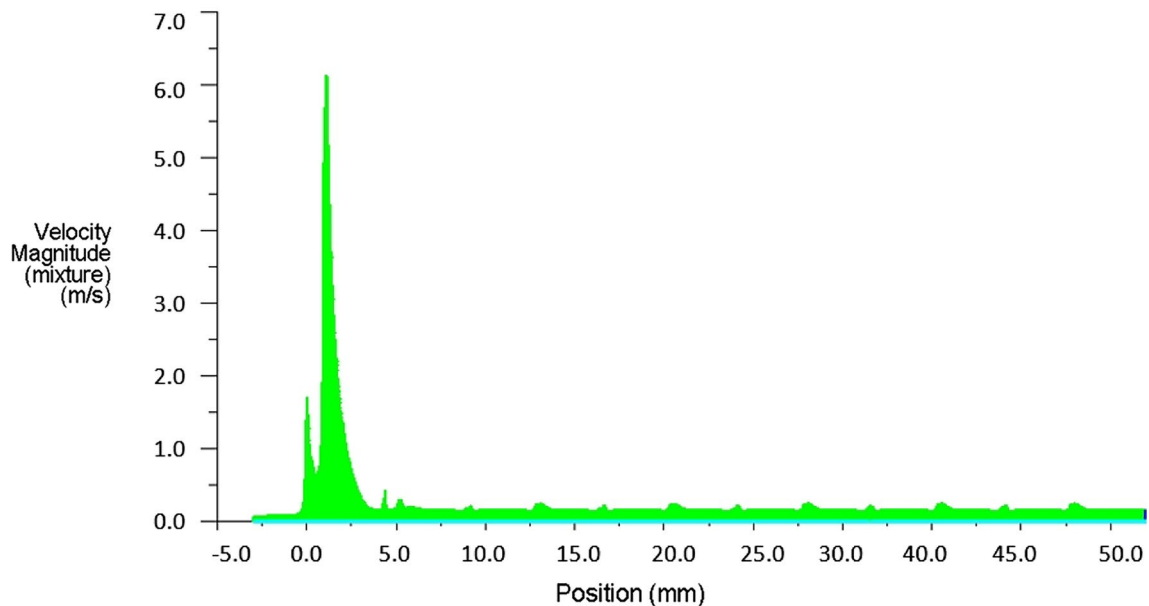
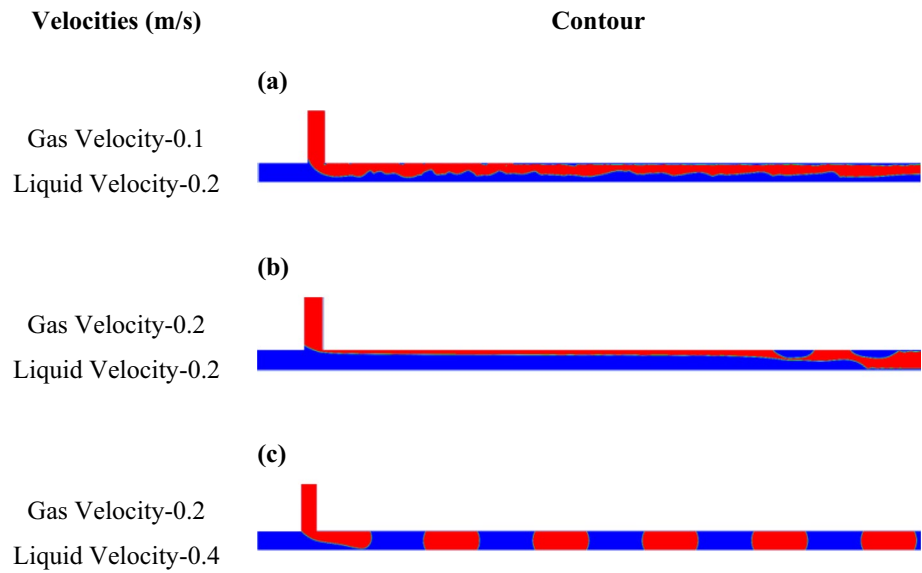


Fig. 11 Velocity fluctuation versus position plot in side T-junction microchannel

is present again at that position. Fluctuation (decreasing and increasing data between 0 and 1) in α value reflects the interface between the CO₂–water system.

Hydrodynamics and mass transfer study of CO₂-different solvent system

Study of hydrodynamics for the diffusive system

Three sets of the simulation were performed for the CO₂-different solvent with the velocities ($u_G=0.2$, and

$u_L=0.4$ m/s) that were obtained in Sect. 3.1 with slug flow pattern. To simulate the present problem ANSYS FLUENT 2021 R2 was used with the solvents water, ethyl alcohol, and ethyl glycol and found that inlet velocities i.e., $u_G=0.2$, and $u_L=0.4$ m/s are suitable condition to gained the slug flow pattern in each case (Table 6).

Extensive experiments were also performed in the laboratory to validate the above results and see the same slug flow pattern in cross-T junction microchannel with almost similar velocities (Table 7). For every case, the formation of each bubble per unit of time is represented in Table 7. In

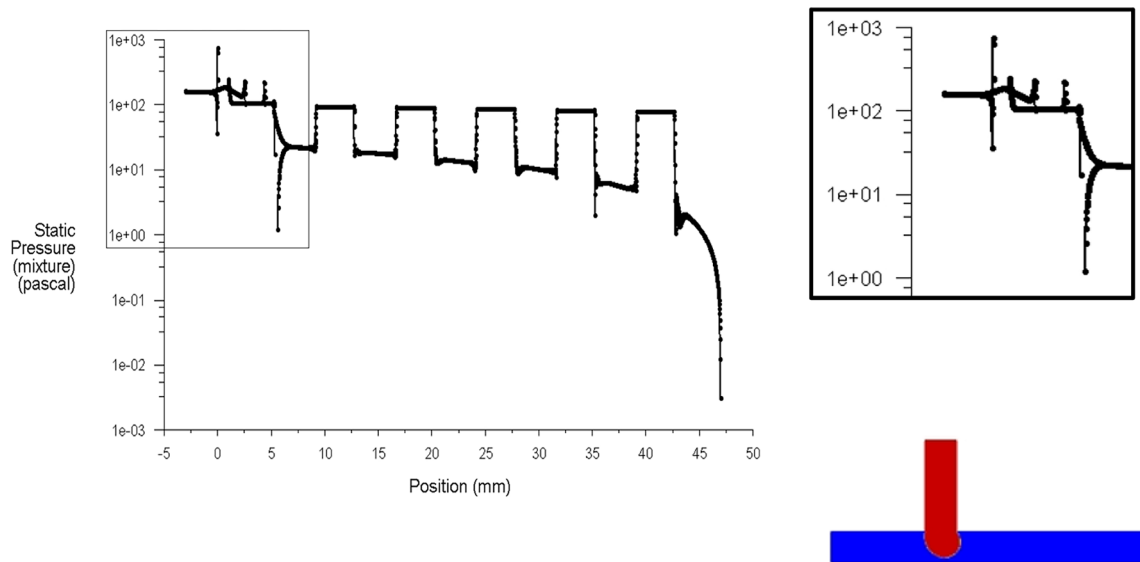


Fig. 12 Representation of pressure fluctuation in the direction of flow

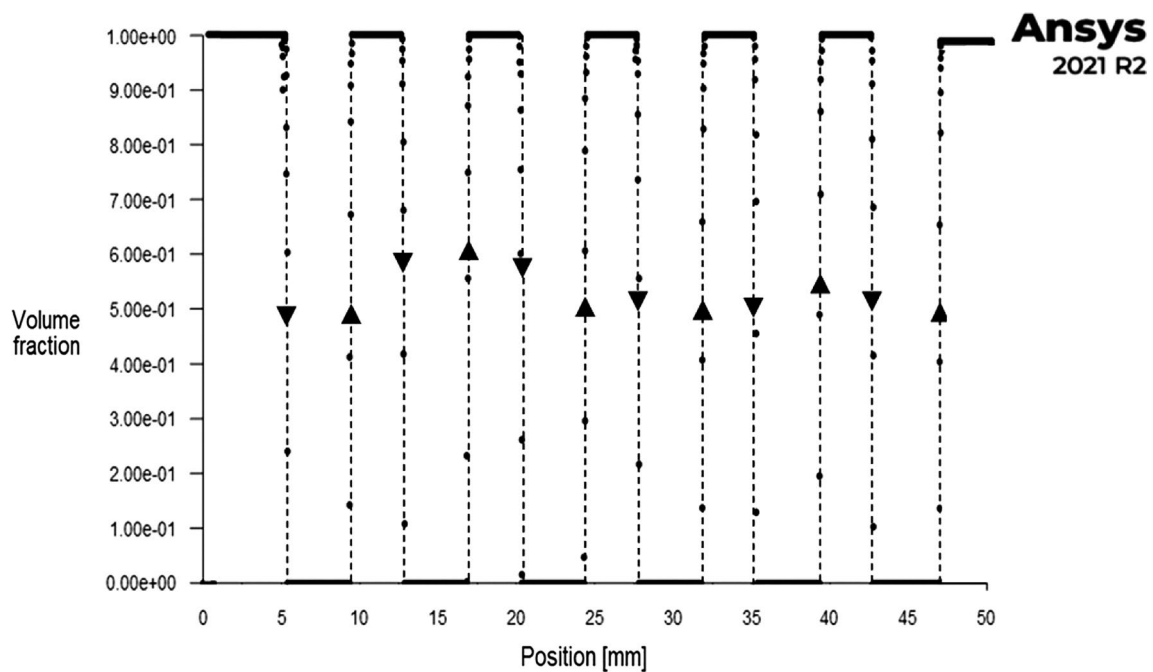


Fig. 13 Variation in the volume fraction plot with the position in the direction of flow

both the approaches (numerical and experimental) one thing is noticeable on the priority that is bubble length decreases.

Calculation of volumetric mass transfer coefficient for the diffusive system

When CO₂ started to pass over the solvents in the micro-channel with slug flow pattern it was observed three different

results for each diffusive system which can be seen in Figs. 16, 17 and Tables 6, 7. As CO₂ began to diffuse in to the liquid, length of the bubble is almost the same for water, ethyl glycol, and has little difference with ethyl-alcohol due to different diffusion rate. It happens because of the presence of hydroxy group and hydrogen bond which inhibit the CO₂ absorption in the solvents. Ethyl Glycol has two hydroxyl groups, while ethyl alcohol and water has just one.

Fig. 14 Movement of the bubble with time when the bubble passes over $x = 19$ mm

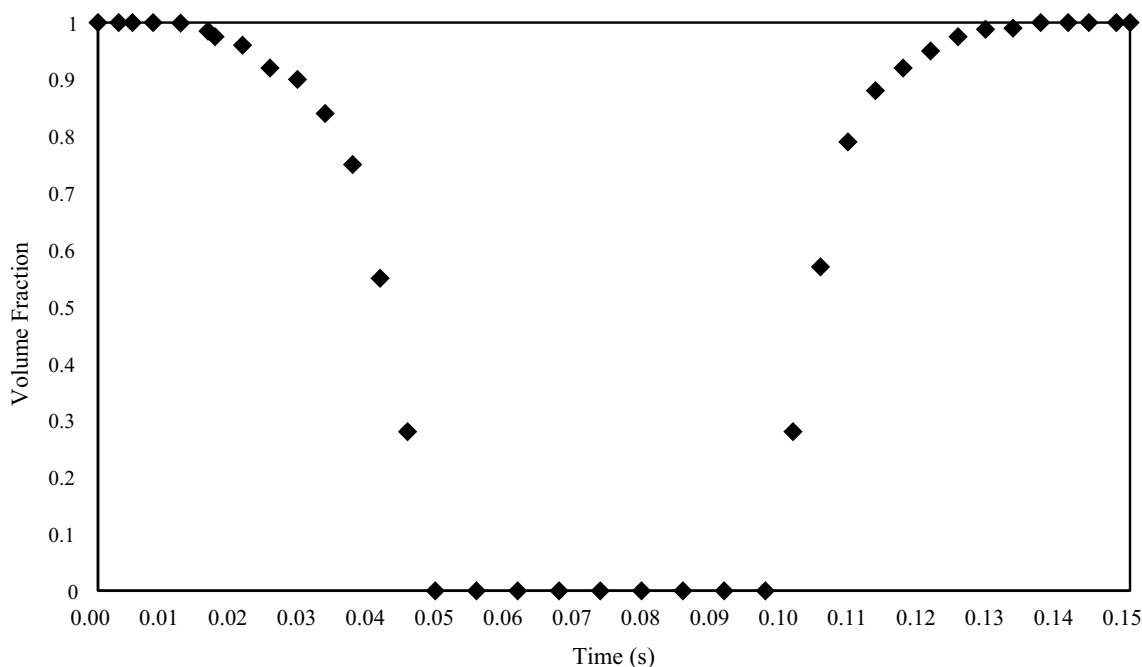
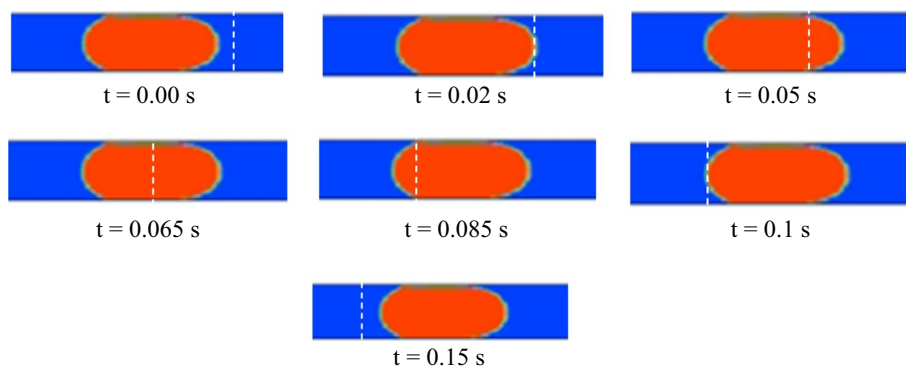


Fig. 15 Change in the value of volume fraction when a bubble passes from $x = 19$ mm

Water also having hydrogen bond which acts as a shield during absorption process. In Figs. 16 and 17, it can be seen clearly that the size of the bubble and the slug reduces with position and in the direction of flow as well and it absorbs in these three solvents in the given order i.e., ethyl alcohol > water > ethyl glycol at temperature (T) = 298.15 K. Basically, solubility of CO_2 into liquid directly affects the bubble size. If the bubble size reduction is faster that represents higher value of volumetric mass transfer coefficient of CO_2 in the solvent. It was also observed that CO_2 -Ethyl Alcohol system having more bubble formation than the other two systems (CO_2 -water and CO_2 -ethyl glycol) in the same cross T-junction microchannel. Presence of a greater number of bubbles in CO_2 -Ethyl Alcohol system reduces the size of slug lengths.

With the help of an experimental data (Figs. 16, 17), it was tried to develop a co-relation between bubble length and its position by finding the unknown terms of Eq. 13 i.e., a, b, and c. The graph was plotted between the measured length of a bubble (during the experiment) and its position by performing non-linear analysis regression curve fitting in MATLAB tool and the obtained values of a, b, and c are listed in Table 8.

Effect of the velocities

To determine the mass transfer coefficient, Eq. 16 (term 'c', including velocity itself) was utilized for each CO_2 -solvent system, experimentally. CO_2 captures in these solvents (water, ethyl alcohol, and ethyl glycol) by physical absorption concept and found that the total volumetric mass transfer

Table 6 Flow pattern contour in the physical absorption process

Case	Fluid	Flow pattern contour
Case-1	CO ₂ -water	
Case-2	CO ₂ -ethyl alcohol	
Case-3	CO ₂ -ethyl glycol	

Table 7 Slug flow pattern obtained for different CO-system experimentally in microreactor

Fluid	Type of flow	Velocities (m/s)	Experimental	Freq (Hz)
CO ₂ -water	Bubbly	$u_G=0.21$ $u_L=0.21$		2
	Slug	$u_G=0.21$ $u_L=0.424$		1
CO ₂ -ethyl Alcohol	Slug	$u_G=0.21$ $u_L=0.424$		1.2
CO ₂ -ethyl Glycol	Slug	$u_G=0.21$ $u_L=0.424$		1

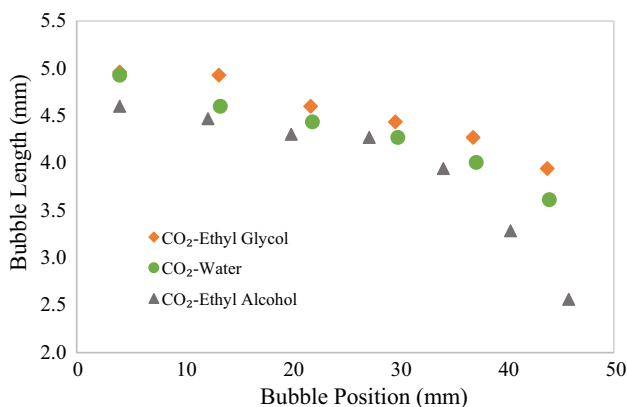


Fig. 16 Effect of the solvents on the length of the bubble

coefficient ($k_L a$) value increases with the bubble velocity and it decreases with the rise of temperature for each case 1, 2, and 3 which is the proper justification of Eq. 16 and diffusion coefficient mention in Table 5. Predicted $k_L a$ values can be arranged for each solvent in decreasing order e.g., ethyl

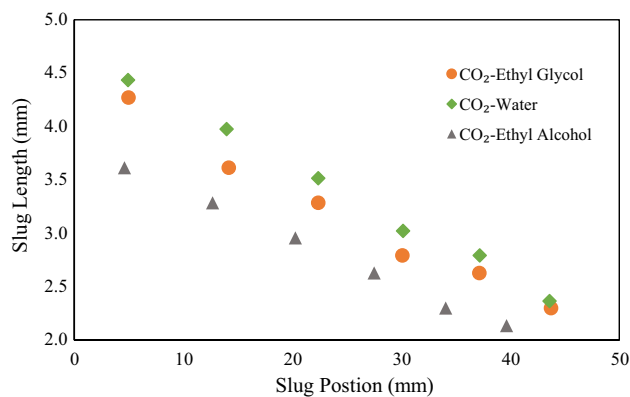


Fig. 17 Effect of the solvents on the slug length

alcohol > water > ethyl glycol (Figs. 18, 19) which follows a similar pattern that from the numerical method in ANSYS FLUENT platform but these values are quite high and listed in Table 9.

Effect of the film thickness

In Eq. 17 it has been seen that the volumetric mass transfer coefficient is a combination of film bubble length side and film bubble cap side coefficients. Here it was tried to observe the dominating factor, either the film length side or cap side in the total volumetric mass transfer coefficient. We developed a model for a single bubble using two film theory concepts in ANSYS Workbench and checked the effect of film thickness on the mass transfer coefficient. Figures 20 and 21 show that the length side coefficient has a much higher value than the cap side mass transfer coefficient (almost negligible) because the interfacial area provided by the length side is much higher for case 1, 2, and 3. It was also found, as the film thickness (δ) increases from 0.01 to 0.05 mm the volumetric mass transfer coefficient started to decrease which is the justification of Eq. 18 at $T = 298.15$ K.

Effect of the solvents

It can be seen from the Figs. 22 and 23 that the volumetric mass transfer coefficient for CO_2 capturing was highest for ethyl alcohol and lowest for ethyl glycol. Further at a fixed temperature, the reduction in the size of the bubble (bubble length) is much higher for ethyl alcohol solvent than the other two solvents that happened because of the different solubilities of CO_2 in these solvents, as discussed above. The reduction in bubble length indicates that some amount

of the gas is transferred to the solvent and the corresponding total volumetric mass transfer coefficient values is comparatively high from those solvents that having relatively large bubble size.

Effect of the temperature

As the temperature increases the solubility of CO_2 in the solvent is decreasing that can be seen in Fig. 24. Table 9 gives sufficient information about the values of total volumetric mass transfer coefficient which was obtained numerically as well as experimentally at $T = 298.15$ K and 303.15 K. Experimental and numerical results were also compared and deviation in the results are represented with the help of Figs. 26 and 27. After successful validation of both the methods it was tried to numerically check the effect of temperature for the large span. From Fig. 25, it can be clearly stated that the total gas–liquid volumetric mass transfer coefficient decreases in CO_2 –ethyl alcohol, CO_2 –water, and CO_2 –ethyl glycol systems with the increase in temperature from 298.15 to 318.15 K. It can be explained as the temperature increases kinetic energy rises. The molecular motion of the gas increases as a result of the greater kinetic energy that breaking intermolecular bonds and molecules started to escape from the solvent and volumetric mass transfer coefficient decreases.

Table 8 Regression coefficient and developed co-relation of bubble length

System	a	b	c	R^2	Length of bubble (mm)
CO_2 –water	3.6	2.41	0.0451	0.991	$L_B = 3.6 + 2.41e^{-0.0451x}$
CO_2 –ethyl alcohol	2.6	5.872	0.067	0.996	$L_B = 2.6 + 5.872e^{-0.0674x}$
CO_2 –ethyl glycol	3.9	1.35	0.0375	0.995	$L_B = 3.9 + 1.35e^{-0.0375x}$

Fig. 18 Effect of the velocities on the bubble length at $T = 298.15$ K

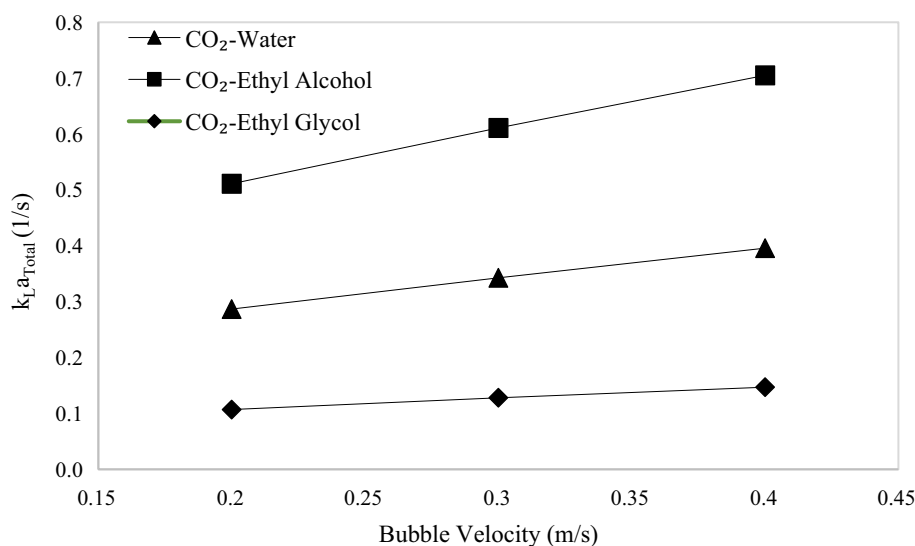


Fig. 19 Effect of the velocities on the bubble length at $T = 303.15\text{ K}$

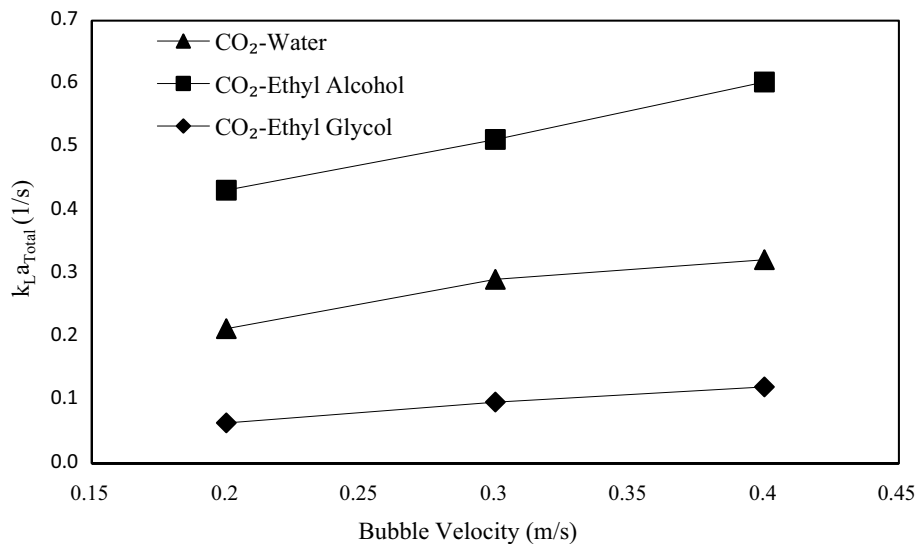


Table 9 k_{La} values data obtained from experiments and simulation at different temperatures and velocities

Temperature (K)	Velocity (m/s)	Volumetric mass transfer coefficient (s^{-1})					
		Numerical			Experimental		
		Case-1	Case-2	Case-3	Case-1	Case-2	Case-3
298.15	0.2	0.295	0.523	0.115	0.287	0.511	0.107
	0.3	0.356	0.627	0.132	0.343	0.611	0.128
	0.4	0.412	0.719	0.153	0.396	0.705	0.147
303.15	0.2	0.223	0.445	0.071	0.213	0.432	0.064
	0.3	0.313	0.523	0.109	0.291	0.512	0.097
	0.4	0.337	0.611	0.132	0.322	0.603	0.121

Fig. 20 Effect of the film thickness on the length side volumetric mass transfer coefficient

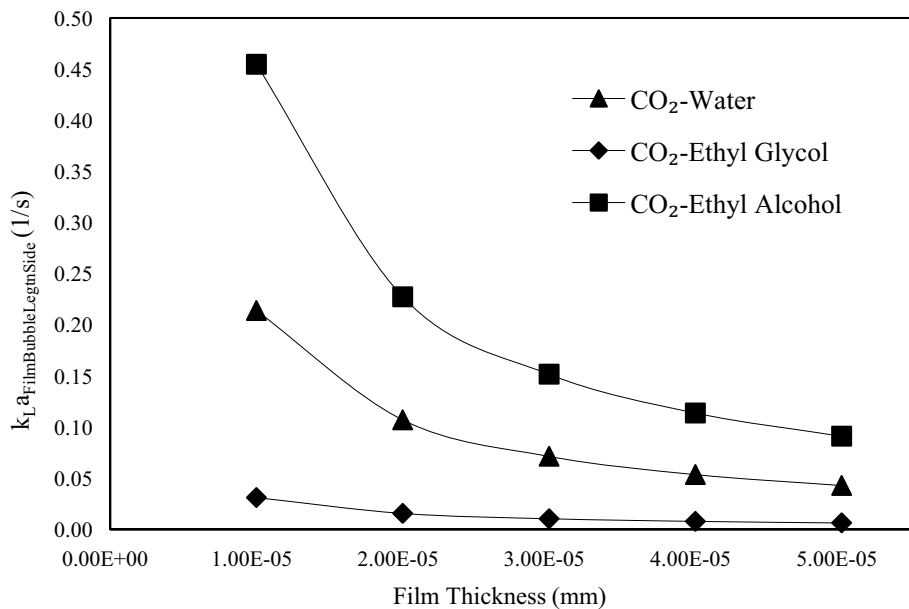


Fig. 21 Effect of the film thickness on the cap side volumetric mass transfer coefficient

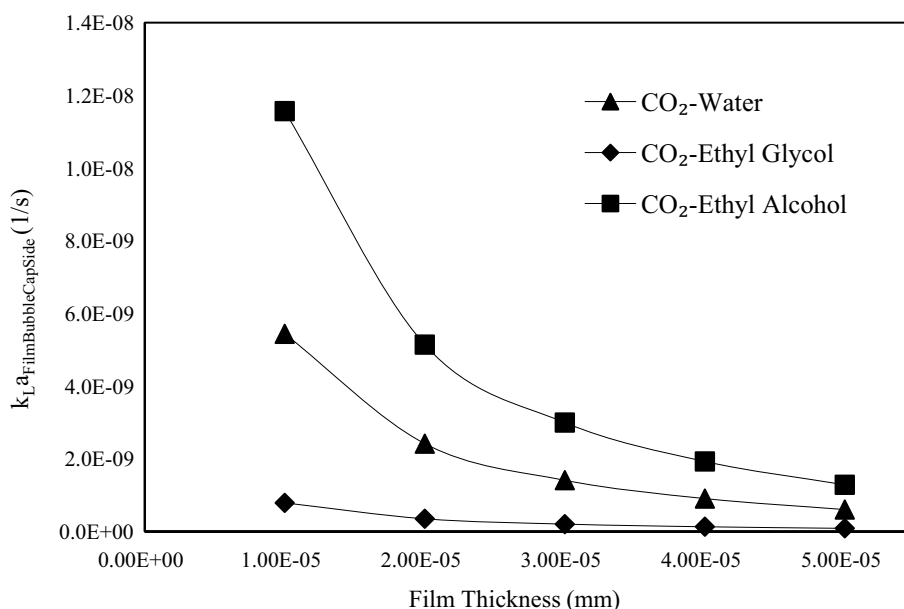
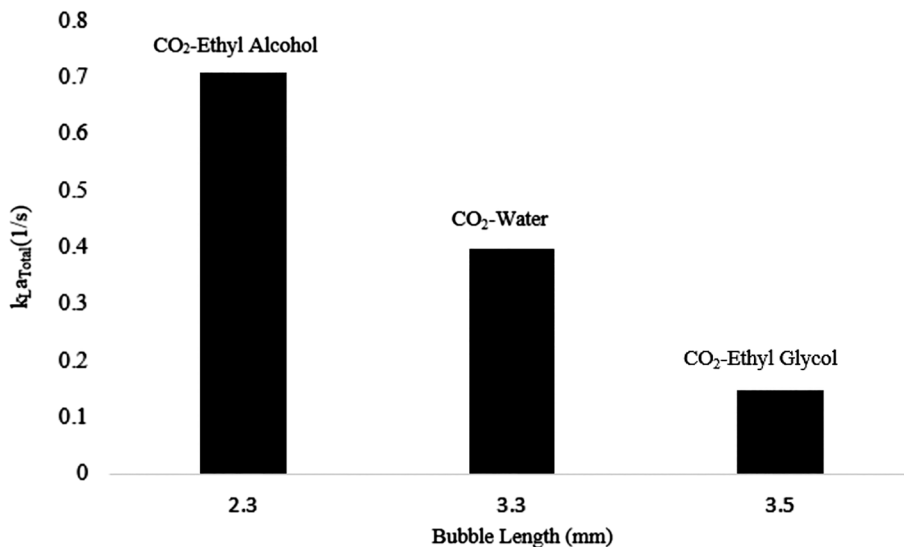


Fig. 22 Effect of the bubble length on the cap side volumetric mass transfer coefficient (T = 298.15 K)



Validation of the results

Total volumetric mass transfer coefficient values obtained numerically are validated with the experimental data at temperature $T = 298.15$ K and 303.15 K and found relative error is approximately 12% and 15% respectively. The data that was obtained from numerical simulation is always higher than the experimental values (Figs. 26, 27). During numerical predictions the value of mass transfer coefficient is always higher than the experimental data as mentioned in Table 9 of the manuscript. The reason behind these predictions is:

1. All the momentum and mass transfer equations were solved at ideal conditions.

2. In real system, ideal assumptions that were considered during simulations are not applicable and real system always deviate with the ideal conditions.
3. During experimental approach some human error (during capturing the bubble image, measuring the length of bubble, fluctuations in the flow rate, and etc.) always be there.

The present work was compared with the literature data for the microchannel as well as the conventional channel. Operating conditions for each system (conventional/microchannels) are listed in Table 10.

In this work, it was found that the current study gives better observations by the use of cross T-junction microchannel than the conventional channel (packed tower) and other

Fig. 23 Effect of the bubble length on the cap side volumetric mass transfer coefficient ($T = 303.15\text{ K}$)

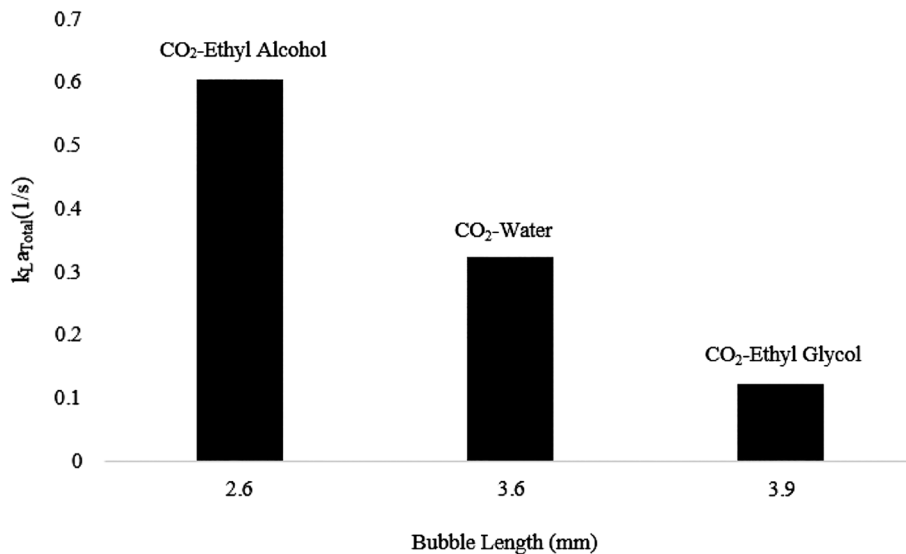


Fig. 24 Effect of the temperature on the volumetric mass transfer coefficient

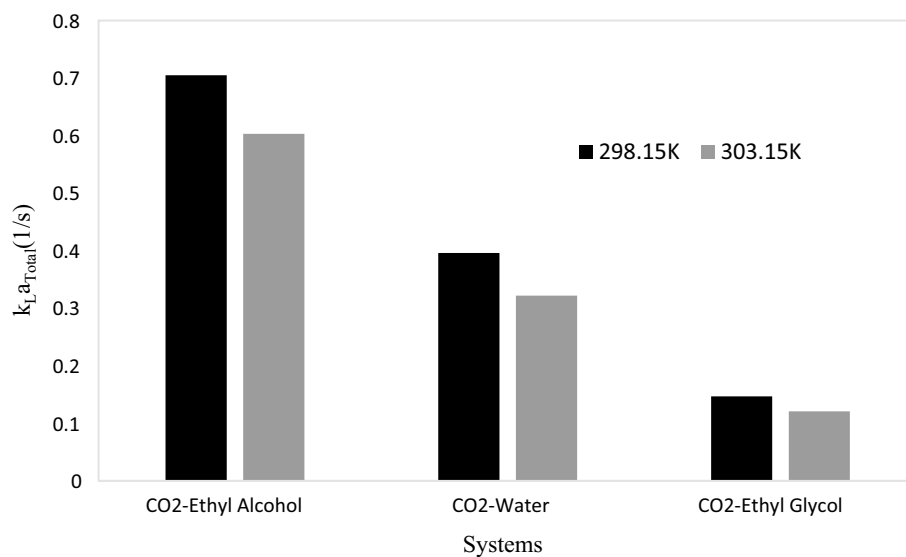


Fig. 25 Numerical results to check effect of the temperature on the volumetric mass transfer coefficient for the values 298.15 K, 303.15 K, 308.15 K, 313.15 K and 318.15 K

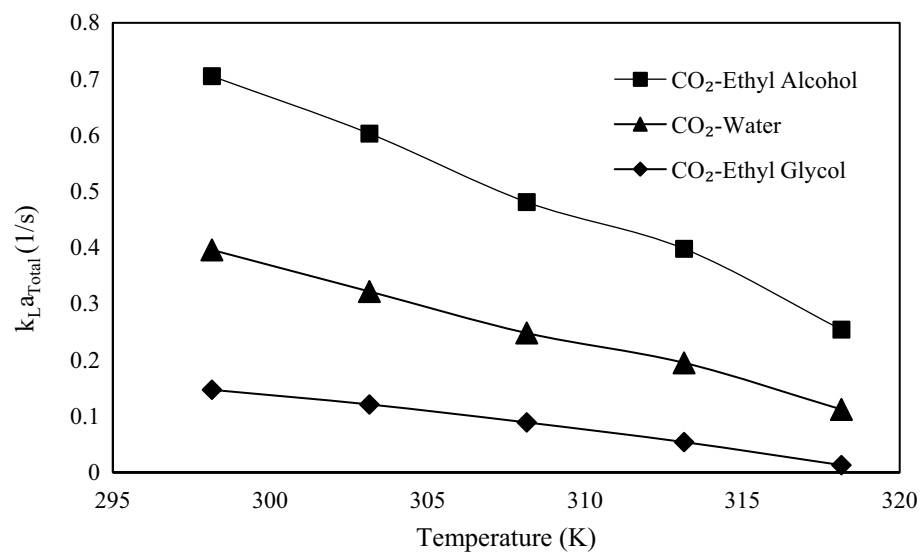


Fig. 26 Comparison of the total volumetric mass transfer coefficient of the present study by both approaches at temperature (T)=298.15 K

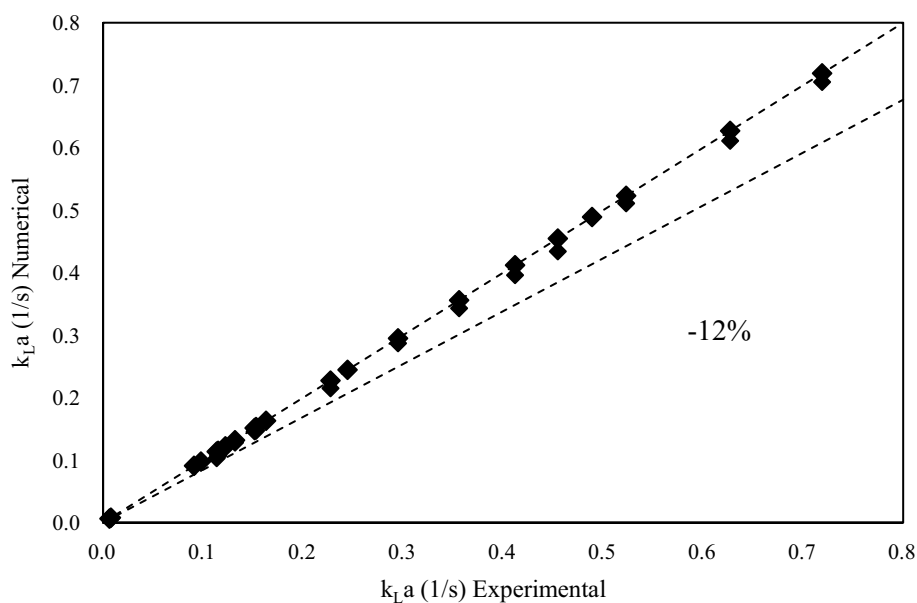
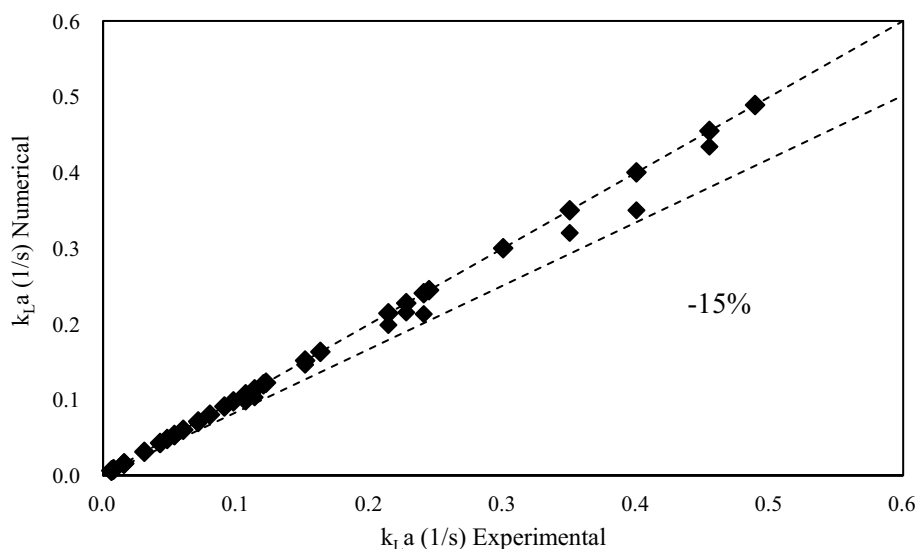


Fig. 27 Comparison of the total volumetric mass transfer coefficient of the present study by both approaches at temperature (T)=303.15 K



types of T-junction orientation with the slug flow pattern (Table 11).

Conclusion

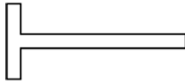

In this article, gas–liquid hydrodynamics (velocity contour, pressure variation, and change in volume fraction) study was performed for CO₂–Water, CO₂–ethyl alcohol, and CO₂–ethyl glycol and total volumetric mass transfer coefficient calculated for a diffusive system by physical absorption in a microchannel. Initially, the velocity range is decided for slug flow pattern in a microchannel with the help of an CO₂–water system using volume of fluid method (VOF) in

numerical simulation and this velocity range was imposed on the diffusive system for the calculation of total mass transfer coefficient. Obtained velocities from the simulation fit for experimental with quite low-velocity data that create the approximately 15% error in the coefficient values. Numerically, two film theory was the base to calculate the film bubble length side and cap side of the bubble volumetric mass transfer coefficient and found that $k_{L,a}^{\text{FilmBubbleLengthSide}}$ value is the major part of the total volumetric mass transfer coefficient. From the experimental data, an empirical correlation was developed for the calculation of bubble size with its position in microchannel and cases 1, 2, and 3 that also helped to calculate the mass transfer coefficient in slug flow. Numerical and experimental results were compared

Table 10 Experimental conditions used for the conventional and microchannels in present study and literature data

References	System	Diameter (mm)	Temperature (K)	Pressure (kPa)	Gas velocity (m.s ⁻¹)
Salimi and Salimi (2016)	CO ₂ -nanofluid	30	298	100	2.18
Zunlong et al. (2021)	CO ₂ -ethanol	0.02	298.15	101.325	0.3
Present work	CO ₂ -Ethanol	1	298.15	101.325	0.4

Table 11 Comparison of total volumetric mass transfer coefficient (s⁻¹) values with present and literature data

References	Salimi and Salimi (2016)	Zunlong et al. (2021)	Present work
Type of channels	Conventional channel	Microchannel (T-junction)	Microchannel (Cross T-junction)
Volumetric mass transfer coefficient (s ⁻¹)	0.005	0.41	0.705
Systems	Packed tower		

and found 15% error with uncontrollable human and equipment errors.

It was observed with the increase of bubble velocities total mass transfer coefficient also increases, and with the film thickness it shows the opposite effect due to dominating parameters in the microchannel i.e., surface tension. With an increase in temperature, the diffusion coefficient started to decrease which slowed down the mass transfer rate. Therefore, mass transfer coefficient values decrease with the slug flow pattern in a cross-T-junction microchannel. For the temperature experimentally (298.15 K and 303.15 K) and numerically (298.15 K and 318.15 K) mass transfer coefficient increases in the given order CO₂-ethyl Glycol, CO₂-water, and CO₂-ethyl alcohol system respectively.

It was also noticed that solvent in the physical absorption process is an important criterion that highly depends on the different functional groups (OH, COO, C=O, -O-, hydrogen bond) and for this work, it was estimated that alcohols have a greater ability to absorb the CO₂ than the hydroxyl group, glycol group, and hydrogen bond.

In conventional, mini, and microchannel, it is found that cross-T junction microchannel provides the higher value of volumetric mass transfer coefficient in the physical absorption process with the slug flow.

Declarations

Conflict of interest The authors declare that they have no known competing financial interests or personal relationships that could have appeared to influence the work reported in this paper. The authors declare that they have no known competing financial interests or personal relationships that could have appeared to influence the work reported in this paper.

References

- Abadie T, Aubin J, Legendre D, Xuereb C (2012) Hydrodynamics of gas-liquid Taylor flow in rectangular microchannels. *Microfluid Nanofluidics* 12(1–4):355–369. <https://doi.org/10.1007/s10404-011-0880-8>
- Adak S, Kundu M, Kundu M (2020) J Pre-proof
- Aghel B, Heidaryan E, Sahraie S, Nazari M (2018) Optimization of monoethanolamine for CO₂ absorption in a microchannel reactor. *J CO₂ Util* 28(July):264–273. <https://doi.org/10.1016/j.jcou.2018.10.005>
- Ahmed R, Liu G, Yousaf B, Abbas Q, Ullah H, Ali MU (2020) Recent advances in carbon-based renewable adsorbent for selective carbon dioxide capture and separation—a review. *J Clean Prod* 242:118409. <https://doi.org/10.1016/j.jclepro.2019.118409>
- Ansari MA, Kim KY, Kim SM (2010) Numerical study of the effect on mixing of the position of fluid stream interfaces in a rectangular microchannel. *Microsyst Technol* 16(10):1757–1763. <https://doi.org/10.1007/s00542-010-1100-2>
- Barzagli F, Giorgi C, Mani F, Peruzzini M (2017) CO₂ capture by aqueous Na₂CO₃ integrated with high-quality CaCO₃ formation and pure CO₂ release at room conditions. *J CO₂ Util* 22(September):346–354. <https://doi.org/10.1016/j.jcou.2017.10.016>
- Bhown AS, Freeman BC (2011) Analysis and status of post-combustion carbon dioxide capture technologies. *Environ Sci Technol* 45(20):8624–8632. <https://doi.org/10.1021/es104291d>
- Bonaventura D, Chacartegui R, Valverde JM, Becerra JA, Verda V (2017) Carbon capture and utilization for sodium bicarbonate production assisted by solar thermal power. *Energy Convers Manag* 149:860–874. <https://doi.org/10.1016/j.enconman.2017.03.042>
- Bordbar A, Taassob A, Zarnaghsh A, Kamali R (2018) Slug flow in microchannels: numerical simulation and applications. *J Ind Eng Chem* 62:26–39. <https://doi.org/10.1016/j.jiec.2018.01.021>
- Boruah MP, Sarker A, Randive PR, Pati S, Chakraborty S (2018) Wettability-mediated dynamics of two-phase flow in microfluidic T-junction. *Phys Fluids* 30:12. <https://doi.org/10.1063/1.5054898>
- Brackbill JU, Kothe DB, Zemach C (1992) A continuum method for modeling surface tension. *J Comput Phys* 100(2):335–354. [https://doi.org/10.1016/0021-9991\(92\)90240-Y](https://doi.org/10.1016/0021-9991(92)90240-Y)
- Buckingham J, Reina TR, Duyar MS (2022) Recent advances in carbon dioxide capture for process intensification. *Carbon Capture Sci*

- Technol 2(November 2021):100031. <https://doi.org/10.1016/j.ccs.2022.100031>
- Chandra AK, Kishor K, Mishra PK, Siraj Alam M (2015) Numerical simulation of heat transfer enhancement in periodic converging-diverging microchannel. *Procedia Eng* 127:95–101. <https://doi.org/10.1016/j.proeng.2015.11.431>
- Chandra AK, Kishor K, Mishra PK, Alam MS (2016) Numerical investigations of two-phase flows through enhanced microchannels. *Chem Biochem Eng Q* 30(2):149–159. <https://doi.org/10.15255/CABEQ.2015.2289>
- Chaoqun Y, Yuchao Z, Chunbo Y, Minhui D, Zhengya D, Guangwen C (2013) Characteristics of slug flow with inertial effects in a rectangular microchannel. *Chem Eng Sci* 95:246–256. <https://doi.org/10.1016/j.ces.2013.03.046>
- Chen G, Yue J, Yuan Q (2008) Gas–liquid microreaction technology: recent developments and future challenges. *Chin J Chem Eng* 16(5):663–669. [https://doi.org/10.1016/S1004-9541\(08\)60138-X](https://doi.org/10.1016/S1004-9541(08)60138-X)
- Chiriac E, Avram M, Balan C (2022) Investigation of multiphase flow in a trifurcation microchannel: a benchmark problem. *Micromachines* 13(6):1–15. <https://doi.org/10.3390/mi13060974>
- Criado YA, Arias B, Abanades JC (2017) Calcium looping CO₂ capture system for back-up power plants. *Energy Environ Sci* 10(9):1994–2004. <https://doi.org/10.1039/c7ee01505d>
- Davison J (2007) Performance and costs of power plants with capture and storage of CO₂. *Energy* 32(7):1163–1176. <https://doi.org/10.1016/j.energy.2006.07.039>
- Dix J, Jokar A (2018) A microchannel heat exchanger for electronics cooling applications Joseph. In: Sixth international ASME conference on nanochannels, microchannels minichannels ICNMM2008, p 2
- Dong C, Hibiki T (2018) Heat transfer correlation for two-component two-phase slug flow in horizontal pipes. *Appl Therm Eng* 141(January):866–876. <https://doi.org/10.1016/j.applthermaleng.2018.06.029>
- Ejaz F, Pao W, Shakir Nasif M, Saieed A, Memon ZQ, Nuruzzaman M (2021) A review: Evolution of branching T-junction geometry in terms of diameter ratio, to improve phase separation. *Eng Sci Technol Int J* 24(5):1211–1223. <https://doi.org/10.1016/j.jestch.2021.02.003>
- Extavour M, Bunje P (2016) CCUS: utilizing CO₂ to reduce emissions | AIChE, pp 1–12. <https://www.aiche.org/resources/publications/cep/2016/june/ccus-utilizing-co2-reduce-emissions>
- Fluent Theory Guide (2013) Ansys fluent theory guide. ANSYS Inc., USA 15317(November), 724–746. <http://scholar.google.com/scholar?hl=en&btnG=Search&q=intitle:ANSYS+FLUENT+Theory+Guide#0>
- Ganguli AA, Pandit AB (2021) Hydrodynamics of liquid–liquid flows in micro channels and its influence on transport properties: a review. *Energies* 14(19):1–56. <https://doi.org/10.3390/en14190666>
- Ghadyanlou F, Azari A, Vatani A (2022) Experimental investigation of mass transfer intensification for CO₂ capture by environment-friendly water based nanofluid solvents in a rotating packed bed. *Sustain*. <https://doi.org/10.3390/su14116559>
- Göttlicher G, Pruschek R (1997) Comparison of CO₂ removal systems for fossil-fuelled power plant processes. *Energy Convers Manag* 38(SUPPL. 1):173–178. [https://doi.org/10.1016/s0196-8904\(96\)00265-8](https://doi.org/10.1016/s0196-8904(96)00265-8)
- Gui X, Tang Z, Fei W (2011) Solubility of CO₂ in alcohols, glycols, ethers, and ketones at high pressures from (288.15 to 318.15) K. *J Chem Eng Data* 56(5):2420–2429. <https://doi.org/10.1021/je101344v>
- Gul A (2022) Effect of temperature and gas flow rate on CO₂ capture 6(2)
- Guo Y, Dong Y, Lei Z, Ma W (2021) Hydrodynamics and gas-liquid mass transfer of CO₂ absorption into [NH₂e-mim][BF₄]-MEA mixture in a monolith channel. *Chem Eng Process Process Intensif* 163(December 2020):108368. <https://doi.org/10.1016/j.cep.2021.108368>
- Harkou E, Hafeez S, Manos G, Constantinou A (2021) CFD study of the numbering up of membrane microreactors for CO₂ capture. *Processes* 9:9. <https://doi.org/10.3390/pr9091515>
- Hayduk W, Malik VK (1971) Density, viscosity, and carbon dioxide solubility and diffusivity in aqueous ethylene glycol solutions. *J Chem Eng Data* 16(2):143–146. <https://doi.org/10.1021/je60049a005>
- Hirt CW, Nichols BD (1981) Volume of fluid (VOF) method for the dynamics of free boundaries. *J Comput Phys* 39(1):201–225. [https://doi.org/10.1016/0021-9991\(81\)90145-5](https://doi.org/10.1016/0021-9991(81)90145-5)
- Huang K, Zhang JY, Hu XB, Wu YT (2017) Absorption of H₂S and CO₂ in aqueous solutions of tertiary-amine functionalized protic ionic liquids. *Energy Fuels* 31(12):14060–14069. <https://doi.org/10.1021/acs.energyfuels.7b03049>
- Huang H et al (2019) Drug-release system of microchannel transport used in minimally invasive surgery for hemostasis. *Drug Des Devel Ther* 13:881–896. <https://doi.org/10.2147/DDDT.S180842>
- IEA (2022) Global energy review: CO₂ emissions in 2021, Iea, pp 1–12. <https://www.iea.org/reports/global-energy-review-co2-emissions-in-2021-2>
- Kang S, Kim H, Kim D (2021) Mitigation of pressure fluctuation in two-phase slug flow by rib geometry. *Int J Multiphase Flow*. <https://doi.org/10.1016/j.ijmultiphaseflow.2021.103753>
- Kenarsari SD et al (2013) Review of recent advances in carbon dioxide separation and capture. *RSC Adv* 3(45):22739–22773. <https://doi.org/10.1039/c3ra43965h>
- Kenig EY, Su Y, Lautenschleger A, Chasanis P, Grünwald M (2013) Micro-separation of fluid systems: a state-of-the-art review. *J Res* 120:245–264
- Khan W, Chandra AK, Kishor K, Sachan S, Alam MS (2018) Slug formation mechanism for air–water system in T-junction microchannel: a numerical investigation. *Chem Pap* 72(11):2921–2932. <https://doi.org/10.1007/s11696-018-0522-7>
- Khan SN, Hailegiorgis SM, Man Z (2017) High pressure solubility of carbon dioxide (CO₂) in aqueous solution of piperazine (PZ) activated N-methyldiethanolamine (MDEA) solvent for CO₂ capture high pressure solubility of carbon dioxide (CO₂) in aqueous solution of piperazine (PZ) act 020081
- Khan W, Sachan S, Alam MS, Khatoun B (2021) Kinetic study of CO₂ capture using amines in conventional and microfluidic devices, September
- Khatoun B, Shabih-Ul-Hasan, Alam MS (2022) Study of mass transfer coefficient of CO₂ capture in different solvents using microchannel: a comparative study. In: Yamashita Y, Kan MBT-CACE (eds) 14 international symposium on process systems engineering, vol 49, pp 691–696. Elsevier
- King MR (2006) Biomedical applications of microchannel flows. *Heat Transf Fluid Flow Minichannels Microchannels* 25:409–442. <https://doi.org/10.1016/B978-008044527-4/50009-8>
- Krauß M, Rzehak R (2017) Reactive absorption of CO₂ in NaOH: detailed study of enhancement factor models. *Chem Eng Sci* 166(March):193–209. <https://doi.org/10.1016/j.ces.2017.03.029>
- Kreutzer MT, Kapteijn F, Moulijn JA, Heiszwolf JJ (2005) Multiphase monolith reactors: chemical reaction engineering of segmented flow in microchannels. *Chem Eng Sci* 60(22):5895–5916. <https://doi.org/10.1016/j.ces.2005.03.022>
- Kuhn S, Jensen KF (2012) A pH-sensitive laser-induced fluorescence technique to monitor mass transfer in multiphase flows in microfluidic devices. *Ind Eng Chem Res* 51(26):8999–9006. <https://doi.org/10.1021/ie300978n>
- Kundu M, Bandyopadhyay SS (2006) Solubility of CO₂ in water + diethanolamine + 2-amino-2-methyl-1-propanol. *J Chem Eng Data* 51(2):398–405. <https://doi.org/10.1021/je050311v>

- Lee AS, Eslick JC, Miller DC, Kitchin JR (2013) Comparisons of amine solvents for post-combustion CO₂ capture: a multi-objective analysis approach. *Int J Greenh Gas Control* 18:68–74. <https://doi.org/10.1016/j.ijggc.2013.06.020>
- Leung DY, Caramanna G, Maroto-Valer MM (2014) An overview of current status of carbon dioxide capture and storage technologies. *Renew Sustain Energy Rev* 39:426–443. <https://doi.org/10.1016/j.rser.2014.07.093>
- Li WL, Liang HW, Wang JH, Shao L, Chu GW, Xiang Y (2022) CFD modeling on the chemical absorption of CO₂ in a microporous tube-in-tube microchannel reactor. *Fuel* 327(15):125064. <https://doi.org/10.1016/j.fuel.2022.125064>
- Lim AE, Lim CY, Lam YC, Lim YH (2019) Effect of microchannel junction angle on two-phase liquid–gas Taylor flow. *Chem Eng Sci* 202:417–428. <https://doi.org/10.1016/j.ces.2019.03.044>
- Liu J, Wang S, Zhao B, Tong H, Chen C (2009) Absorption of carbon dioxide in aqueous ammonia. *Energy Procedia* 1(1):933–940. <https://doi.org/10.1016/j.egypro.2009.01.124>
- Liu D, Ling X, Peng H (2016) Comparative analysis of gas–liquid flow in T-junction microchannels with different inlet orientations. *Adv Mech Eng* 8(3):1–14. <https://doi.org/10.1177/16878140166637329>
- Mahmoudi Marjanian M, Shahhosseini S, Ansari A (2021) Investigation of the ultrasound assisted CO₂ absorption using different absorbents. *Process Saf Environ Prot* 149:277–288. <https://doi.org/10.1016/j.psep.2020.10.054>
- Makarem MA, Farsi M, Rahimpour MR (2021) CFD simulation of CO₂ removal from hydrogen rich stream in a microchannel. *Int J Hydrog Energy* 46(37):19749–19757. <https://doi.org/10.1016/j.ijhydene.2020.07.221>
- Mastiani M, Mosavati B, Kim M (2017) Numerical simulation of high inertial liquid-in-gas droplet in a T-junction microchannel. *RSC Adv* 7(77):48512–48525. <https://doi.org/10.1039/c7ra09710g>
- Ministry of earth sciences nowcast specialized forecasts climate services— anomaly time series of temperature & rainfall climate of smart cities, p 31
- Modak A, Jana S (2019) Advancement in porous adsorbents for post-combustion CO₂ capture. *Microporous Mesoporous Mater* 276(September):107–132. <https://doi.org/10.1016/j.micromeso.2018.09.018>
- Mukherjee A, Okolie JA, Abdelrasoul A, Niu C, Dalai AK (2019) Review of post-combustion carbon dioxide capture technologies using activated carbon. *J Environ Sci (china)* 83:46–63. <https://doi.org/10.1016/j.jes.2019.03.014>
- Nekouei M, Vanapalli SA (2017) Volume-of-fluid simulations in microfluidic T-junction devices: influence of viscosity ratio on droplet size Mehdi Nekouei and Siva A. Vanapalli Department of Chemical Engineering, Texas Tech University, Lubbock, TX, 79409, USA, vol 032007, pp 1–22
- Ni D, Hong FJ, Cheng P, Chen G (2017) Numerical study of liquid–gas and liquid–liquid Taylor flows using a two-phase flow model based on Arbitrary–Lagrangian–Eulerian (ALE) formulation. *Int Commun Heat Mass Transf* 88(September):37–47. <https://doi.org/10.1016/j.icheatmasstransfer.2017.08.006>
- Ochedi FO, Liu Y, Adewuyi YG (2020) State-of-the-art review on capture of CO₂ using adsorbents prepared from waste materials. *Process Saf Environ Prot* 139:1–25. <https://doi.org/10.1016/j.psep.2020.03.036>
- Palo DR, Stenkamp VS, Dagle RA, Jovanovic GN (2006) Industrial applications of microchannel process technology in the United States. *J Res* 5:387–414. <https://doi.org/10.1002/9783527616749.ch13>
- Pham H, Wen L, Zhang H (2012) Numerical simulation and analysis of gas–liquid flow in a T-junction microchannel. *Adv Mech Eng*. <https://doi.org/10.1155/2012/231675>
- Pohar A, Plazl I (2009) Process intensification through microreactor application. *Chem Biochem Eng Q* 23(4):537–544
- Pua LM, Rumbold SO (2003) Industrial microchannel devices: where are we today? *Int Conf Microchannels Minichannels* 1:773–780. <https://doi.org/10.1115/icmm2003-1101>
- Qian D, Lawal A (2006) Numerical study on gas and liquid slugs for Taylor flow in a T-junction microchannel. *Chem Eng Sci* 61(23):7609–7625. <https://doi.org/10.1016/j.ces.2006.08.073>
- Ramdin M, De Loos TW, Vlucht TJH (2012) State-of-the-art of CO₂ capture with ionic liquids. *Ind Eng Chem Res* 51(24):8149–8177. <https://doi.org/10.1021/ie3003705>
- Rastegar Z, Ghaemi A (2022) CO₂ absorption into potassium hydroxide aqueous solution: experimental and modeling. *Heat Mass Transf Und Stoffuebertragung* 58(3):365–381. <https://doi.org/10.1007/s00231-021-03115-9>
- Renken A, Kiwi-Minsker L (2010) Microstructured catalytic reactors. *Adv Catal* 53(C):47–122. [https://doi.org/10.1016/S0360-0564\(10\)53002-5](https://doi.org/10.1016/S0360-0564(10)53002-5)
- Rodríguez-Mosqueda R, Bramer EA, Brem G (2018) CO₂ capture from ambient air using hydrated Na₂CO₃ supported on activated carbon honeycombs with application to CO₂ enrichment in greenhouses. *Chem Eng Sci* 189:114–122. <https://doi.org/10.1016/j.ces.2018.05.043>
- Rouzitab Z, Maklavany DM, Jafarinejad S, Rashidi A (2020) Lignocellulose-based adsorbents: a spotlight review of the effective parameters on carbon dioxide capture process. *Chemosphere* 246:125756. <https://doi.org/10.1016/j.chemosphere.2019.125756>
- Salimi J, Salimi F (2016) CO₂ capture by water-based Al₂O₃ and Al₂O₃–SiO₂ mixture nanofluids in an absorption packed column. *Rev Mex Ing Quim* 15(1):185–192
- Santos RM, Kawaji M (2011) Gas–liquid slug formation at a rectangular microchannel T-junction: a CFD benchmark case. *Cent Eur J Eng* 1(4):341–360. <https://doi.org/10.2478/s13531-011-0038-1>
- Sarkar S, Singh KK, Shankar V, Shenoy KT (2014) Numerical simulation of mixing at 1–1 and 1–2 microfluidic junctions. *Chem Eng Process Process Intensif* 85:227–240. <https://doi.org/10.1016/j.cep.2014.08.010>
- Simons J, Ponter AB, Simons J, Ponter AB (1975) Diffusivity of carbon dioxide in ethanol–water mixtures. *J Chem Eng Jpn* 8(5):347–350. <https://doi.org/10.1252/jcej.8.347>
- Snijder ED, Riele MJM, Versteeg GF, Van Swaaij WPM (1996) Diffusion coefficients of CO, COS, pp 37–39
- Souvignet I, Olesik SV (1998) Molecular Diffusion coefficients in ethanol/water/carbon dioxide mixtures. *Anal Chem* 70(14):2783–2788. <https://doi.org/10.1021/ac971263n>
- Tan LS, Shariff AM, Lau KK, Bustam MA (2012) Factors affecting CO₂ absorption efficiency in packed column: a review. *J Ind Eng Chem* 18(6):1874–1883. <https://doi.org/10.1016/j.jiec.2012.05.013>
- Triplett KA, Ghiaasiaan SM, Abdel-Khalik SI, Sadowski DL (1999) Gas–liquid two-phase flow in microchannels part I: two-phase flow patterns. *Int J Multiph Flow* 25(3):377–394. [https://doi.org/10.1016/S0301-9322\(98\)00054-8](https://doi.org/10.1016/S0301-9322(98)00054-8)
- Tuckerman DB, Pease RFW (1981) High-performance heat sinking for VLSI. *IEEE Electron Dev Lett EDL-2*(5):126–129. <https://doi.org/10.1109/EDL.1981.25367>
- van Baten JM, Krishna R (2011) Corrigendum to ‘CFD simulations of mass transfer from Taylor bubbles rising in circular capillaries’ [Chem. Eng. Sci. 59 (2004) 2535–2545]. *Chem Eng Sci* 66(20):4941. <https://doi.org/10.1016/j.ces.2011.06.064>
- Venkateshwarlu A, Bharti RP (2023) Effects of surface wettability and flow rates on the interface evolution and droplet pinch-off mechanism in the cross-flow microfluidic systems Effects of surface wettability and flow rates on the interface evolution and droplet pinch-off mechanism in the. *Chem Eng Sci* 267(3):118279. <https://doi.org/10.1016/j.ces.2022.118279>
- Wang J, Li H, Li X, Cong H, Gao X (2021) An intensification of mass transfer process for gas–liquid counter-current flow in a novel

- microchannel with limited path for CO₂ capture. *Process Saf Environ Prot* 149:905–914. <https://doi.org/10.1016/j.psep.2021.03.046>
- Yang L, Tan J, Wang K, Luo G (2014) Mass transfer characteristics of bubbly flow in microchannels. *Chem Eng Sci* 109:306–314. <https://doi.org/10.1016/j.ces.2014.02.004>
- Yao C, Dong Z, Zhao Y, Chen G (2014) An online method to measure mass transfer of slug flow in a microchannel. *Chem Eng Sci* 112:15–24. <https://doi.org/10.1016/j.ces.2014.03.016>
- Ye C, Dang M, Yao C, Chen G, Yuan Q (2013) Process analysis on CO₂ absorption by monoethanolamine solutions in microchannel reactors. *Chem Eng J* 225:120–127. <https://doi.org/10.1016/j.cej.2013.03.053>
- Yin Y et al (2022) Effect of solvent on CO₂ absorption performance in the microchannel. *J Mol Liq* 357:119133. <https://doi.org/10.1016/j.molliq.2022.119133>
- Yoro KO, Daramola MO (2020) CO₂ emission sources, greenhouse gases, and the global warming effect. *Adv Carbon Capture* 25:3–28. <https://doi.org/10.1016/b978-0-12-819657-1.00001-3>
- Yue J, Chen G, Yuan Q, Luo L, Gonthier Y (2007) Hydrodynamics and mass transfer characteristics in gas–liquid flow through a rectangular microchannel. *Chem Eng Sci* 62(7):2096–2108. <https://doi.org/10.1016/j.ces.2006.12.057>
- Zhang C, Song W, Ma Q, Xie L, Zhang X, Guo H (2016) Enhancement of CO₂ capture on biomass-based carbon from black locust by KOH activation and ammonia modification. *Energy Fuels* 30(5):4181–4190. <https://doi.org/10.1021/acs.energyfuels.5b02764>
- Zhang Z, Cai J, Chen F, Li H, Zhang W, Qi W (2018) Progress in enhancement of CO₂ absorption by nanofluids: a mini review of mechanisms and current status. *Renew Energy* 118:527–535. <https://doi.org/10.1016/j.renene.2017.11.031>
- Zunlong J, Yonghao L, Rui D, Dingbiao W, Xiaotang C (2021) Numerical study on gas–liquid two-phase flow and mass transfer in a microchannel. *Int J Chem React Eng* 19(3):295–308. <https://doi.org/10.1515/ijcre-2020-0162>

Publisher's Note Springer Nature remains neutral with regard to jurisdictional claims in published maps and institutional affiliations.

Springer Nature or its licensor (e.g. a society or other partner) holds exclusive rights to this article under a publishing agreement with the author(s) or other rightsholder(s); author self-archiving of the accepted manuscript version of this article is solely governed by the terms of such publishing agreement and applicable law.